

NOVEL NANO-LITER SCALE MICROFLUIDIC PLATFORM  
FOR PROTEIN KINETICS

Except where reference is made to the work of others, the work described in this thesis is my own or was done in collaboration with my advisory committee. This thesis does not include propriety or classified information.

---

Sachin Ranappa Jambovane

Certificate of Approval:

---

Jeffrey W. Fergus  
Associate Professor  
Materials Engineering

---

Jong Wook Hong, Chair  
Assistant Professor  
Materials Engineering

---

Barton C. Prorok  
Associate Professor  
Materials Engineering

---

Evert C. Duin  
Assistant Professor  
Chemistry and Biochemistry

---

George T. Flowers  
Interim Dean  
Graduate School

NOVEL NANO-LITER SCALE MICROFLUIDIC PLATFORM  
FOR PROTEIN KINETICS

Sachin Ranappa Jambovane

A Thesis  
Submitted to  
the Graduate Faculty of  
Auburn University  
in Partial Fulfillment of the  
Requirements for the  
Degree of  
Master of Science

Auburn, Alabama  
December 19, 2008

NOVEL NANO-LITER SCALE MICROFLUIDIC PLATFORM FOR  
PROTEIN KINETICS

Sachin Ranappa Jambovane

Permission is granted to Auburn University to make copies of this thesis at its discretion, upon request of individuals or institutions and at their expense. The author reserves all publication rights.

---

Signature of Author

---

Date of Graduation

## VITA

Sachin Ranappa Jambovane, son of Sri. Ranappa Jambovane and Smt. Kasturi Jambovane, was born on March 9, 1976, in Maharashtra, India. He completed his Bachelor of Engineering (Mechanical Engineering) degree from Government College of Engineering, Karad, India in 1998. Then he finished his Master of Technology degree in Mechanical Design Engineering from the prestigious Indian Institute of Technology, Bombay, India, in January 2000. From March 2000 to October 2002, he worked at the Research and development division of The Automotive Research Association of India, Pune in the capacity of Research Engineer and Project Engineer. In Oct 2002, he moved to V.J. Coresoft Pvt. Ltd, (A Subsidiary of Casicorp Inc., USA), India, as a Team leader (Computer Aided Engineering). In August 2003, he entered the Graduate School at Auburn University to pursue a Doctor of Philosophy degree in Mechanical Engineering. In January 2006, he changed his research area to microfluidics, to pursue Master of Science degree in Materials Engineering. In December 2004, he married to Seema Kamble, daughter of Sri. Laxmanrao Kamble and Smt. Sagar Kamble.

THESIS ABSTRACT

NOVEL NANO-LITER SCALE MICROFLUIDIC PLATFORM FOR  
PROTEIN KINETICS

Sachin Ranappa Jambovane

Master of Science, December 19, 2008  
(M. Tech., Indian Institute of Technology Bombay, India, 2000  
B.E., Shivaji University Kolhapur, India, 1998)

109 Typed Pages

Directed by Jong Wook Hong

In the mid-1970s, integrated circuits exploited miniaturized transistors to bring a revolution in the field of computation. This marked the foundation of computers and information technology. In this century, we are on the brink of a similar revolution in the large-scale automation of biological/chemical material processing with nano/microfluidic chips, in the form of a lab-on-a-chip. Lab-on-a-chip is a miniaturized device that manipulates tiny amounts of volumes in micro/nanometer scale channels to automate and integrate many materials processing steps on a single chip.

The advantages of conducting materials processing on a lab-on-a-chip include reduced consumption of reagents, shorter analysis time, greater sensitivity, portability that allows *in situ* and real-time analysis, and easy disposability. Although lab-on-a-chip has many advantages, its successful development is still a challenging task. Recent progress in the area of lab-on-a-chip would impact the area of genomics and proteomics research and hence ultimately the very way we live in today's world.

As engineers are starting to design such compact devices, they are attracting new applications in biotechnology, medicine, point-of-care diagnostics and environmental monitoring. However, current lab-on-a-chip designs have several limitations in terms of conducting complex biomaterial analysis and its parallel processing.

In this thesis, design, development, validation, and testing of a novel microfluidic device to conduct protein kinetics are presented. The microfluidic platform, called a 'protein kinetics chip', can also be used for biological and chemical material processing where reagent gradient generation and parallel processing are required. However, the emphasis is placed on performing enzyme kinetic reactions on a chip. The protein kinetics chip automates the process of metering, concentration gradient generation, mixing, and optical detection. In addition, the chip is comprised of numbers of parallel processors which have the capability to conduct multiple processes simultaneously.

## ACKNOWLEDGEMENTS

The author would like to thank his advisor Dr. Jong Wook Hong, who has helped the author immensely. The author would like to extend a special thanks to Dr. Hong for his devotion, guidance, and mentorship throughout all phases of this research. The author is sincerely thankful to Dr. Evert C. Duin for all his time and guidance in explaining critical issues about experimental and theoretical enzyme kinetics. The author is also thankful to Dr. Jeffrey W. Fergus and Dr. Barton C. Prorok for agreeing to be on his thesis committee. In addition, it was sheer joy to go through the courses taught by them. The author would also like to thank Mr. Charles Ellis of Alabama Microelectronics Science and Technology Center (AMSTC) for permission to use the clean room for microfabrication work. The author would also like to acknowledge the company of his past and current research group members. The author would also like to mention the names of Dr. Jae Young Yun and Dr. Duckjong Kim, for providing valuable input during the course of this project. The author would also like to thank Madhumati Ramanathan, Shankar Balasubramanian, Rigved Epur and Tony Jefferson for allowing the author to use few instruments in their lab. Finally, none of this research would have been possible without the love and support of the author's family and friends: Sri Ranappa Jambovane, Smt. Kasturi Jambovane, Seema Jambovane, Megha Jambovane, Omkar Jambovane, Ramesh Nipanal, Ashok Nipanal, Laxmanrao Kamble, Sagar Kamble, Sudhir Kamble,

Uday Sorte, Naveen Singh, Anjani Kumar, Nilimini Vishwaprakash, Pradeep Rao,  
Kalpesh Shatye, Prasanthi Pallapu, Amol Thote, Gautham Jeppu, Kailash Jajam, Vishal  
Srivastav and Santosh Angadi.



Style manual or journal used Auburn University Graduate School Guide to Preparation of Master's Thesis

Computer software used Microsoft Word, Microsoft Excel, Microsoft Visio, Sigmaplot, Origin Paint, and Adobe Acrobat,

## TABLE OF CONTENTS

LIST OF TABLES .....	xi
LIST OF FIGURES .....	xiii
Chapter One .....	1
INTRODUCTION .....	1
1.1 Background .....	1
1.2 Lab-on-a-chip (LOC) .....	2
1.3 History of Lab-on-a-chip .....	3
1.4 Multilayer Soft Lithography (MSL) .....	5
1.5 Microfluidics .....	10
1.6 Microfluidic pneumatic valve .....	11
1.7 Microfluidic pneumatic Peristaltic mixer .....	14
1.8 Enzyme Kinetics .....	18
1.8.1 Enzymes .....	18
1.8.2 The mechanism of enzyme catalyzed reaction .....	19
1.8.3 Steady state kinetics .....	21
1.9 Organization of Thesis .....	26
Chapter Two .....	27
LITERATURE REVIEW .....	27
2.1 Introduction .....	27
2.2 Microchannel and chamber based fluidic systems .....	28
2.3 Droplet-based microfluidic systems .....	31
2.4 Microwell-based fluidic systems .....	34
2.5 Research Objectives .....	36
Chapter Three .....	38
PROTEIN KINETIC CHIP: .....	38
DEVICE DEVELOPMENT, AND VALIDATION, .....	38
3.1 Introduction .....	38
3.2 Device Design .....	39
3.2.1 Benchmark design scheme .....	39
3.2.2 Protein kinetics chip design Version. 1 .....	41
3.2.3 Protein kinetics chip design Version. 2 .....	42
3.2.4 Protein kinetics chip design Version. 3 .....	42

3.3	Mold Fabrication.....	44
3.4	Chip Fabrication.....	49
3.5	Development OF LabVIEW® control Program .....	54
3.6	Device Validation .....	55
3.7	Conclusion .....	58
	Chapter Four .....	59
	PROTEIN KINETIC CHIP: .....	59
	DEVICE TESTING WITH A MODEL ENZYME SYSTEM .....	59
4.1	Introduction.....	59
4.2	Model enzyme system.....	59
4.4.1	Restrictions on the selection of model enzyme system .....	59
4.4.2	LDH-Diaphorase model enzyme system .....	60
4.4.3	$\beta$ -galactosidase model enzyme system .....	61
4.2	Reagents for chip testing.....	62
4.3	Chip scanning.....	63
4.4	Data analysis .....	64
4.4.1	Standard curve for resorufin .....	65
4.4.2	$\beta$ -galactosidase enzyme-catalyzed on-chip reaction.....	67
4.5	Results.....	71
4.6	Conclusion .....	73
4.7	Scientific issues.....	74
	Chapter Five.....	76
	OVERALL CONCLUSIONS.....	76
5.1	Conclusions of the research .....	76
	Referneces.....	78
	Appendix A.....	82
	Appendix B.....	84
	Appendix C.....	88

## LIST OF TABLES

Table 1.1 : Comparison of Young's moduli of PDMS and other common MEMS materials.....	6
Table 1.2 : Sequence of valve operation for peristaltic motion.....	16
Table 3.1 : Summary of operational scheme of protein kinetics chip.....	40
Table 3.2 : Summary of dye experiment for the validation of working of protein kinetics chip.....	58
Table 4.1 Summary of reagents for protein kinetics chip testing.....	62
Table 4.2 Summary of curve-fitting of $\beta$ -galactosidase enzymatic reaction in order to determine kinetic parameters for $\beta$ -galactosidase on-chip experiment.....	73
Table 4.3 Summary of kinetic parameters for $\beta$ -galactosidase enzyme.....	73

## LIST OF FIGURES

Figure 1.1 : Pictorial history of the developments in the area of microelectronics and .....	4
Figure 1.2 : Revolution from conventional enzyme kinetics experiment to protein kinetics chip.....	5
Figure 1.3 : Chemical structure of Silicone rubber or .....	9
Figure 1.4 : Size characteristics of protein kinetics chip in relation with other objects. ...	11
Figure 1.5 : Schematic of valve closing for square and rounded channels.....	12
Figure 1.6 : Schematic of valve closing for square and rounded channels. The dotted lines designate the contour of the membrane in the rectangular (left) and rounded (right) channel as pressure is applied. ....	13
Figure 1.7 : Schematics of the working of a pneumatically operated peristaltic micromixer.....	15
Figure 2.1 : Schematic of the enzyme analysis chip.....	28
Figure 2.2 : (A) Schematic illustration of the microfluidic device used for analysis of enzyme kinetics. (B) Optical image of a microchamber after packing with microbeads. ....	30
Figure 2.3 : (A) Schematic illustration of single enzyme assay in the microfluidic device. ....	31

Figure 3.1 : Summary of process followed during development of protein kinetics chip.	39
Figure 3.2 : Schematics of operational scheme of protein kinetics chip. ....	41
Figure 3.3 : Design versions of protein kinetics chip. ....	43
Figure 3.4 : Process flow diagram showing mold fabrication process during development of protein kinetics chip.....	45
Figure 3.5 : Flow diagram showing chip fabrication process during development of protein kinetics chip. ....	50
Figure 3.6 : Dye-filled protein kinetics chip with US quarter coin for size .....	52
Figure 3.7 : Cut-section of the protein kinetics chip for the measurement of (a)control channel height;(b)membrane thickness and (c)fluidic channel height.....	53
Figure 3.8 : GUI of LabVIEW <sup>®</sup> program utilized for operating the .....	54
Figure 3.9 : Block diagrams of LabVIEW program utilized for operating the protein kinetics chip; (a) Valve control., (b) Mixer control .....	55
Figure 3.10 : Schematics of the experimental setup for validating the working of the protein kinetic chip. ....	56
Figure 3.11 : The validation of chip operations by using blue, red and yellow colored food dye solutions. ....	57
Figure 4.1 : $\beta$ -Galactosidase enzyme-catalyzed reaction with Resorufin- $\beta$ -D-Galactopyranoside as substrate. ....	62
Figure 4.2 : Experimental set up for fluorescence scanning of the protein kinetics chip.	64
Figure 4.3 : Summary of steps followed during data analysis.....	64
Figure 4.4 : Experiment for resorufin fluorescence standard curve ;(a),Resorufin	

fluorescence (b) Resorufin fluorescence gradient before mixing,(c) Final resorufin fluorescence gradient after the mixing.....	65
Figure 4.5 : Standard curve for resorufin generated by using protein kinetics chip.....	67
Figure 4.6 : Array of scanned pictures generated by scanning the protein kinetics chip.	68
Figure 4.7 : Time history for $\beta$ -galactosidase enzyme obtained by using protein kinetics chip.....	69
Figure 4.8 : Time history in linear kinetics range for $\beta$ -galactosidase enzyme obtained by using protein kinetics chip. ....	70
Figure 4.9 : Initial velocity plot for $\beta$ -galactosidase enzyme obtained by using protein kinetics chip. ....	71
Figure 4.10 : Michaelis-Menten plot for $\beta$ -galactosidase enzyme by using protein kinetics chip.....	72

## **CHAPTER ONE**

### **INTRODUCTION**

#### **1.1 BACKGROUND**

All life, from viruses to human beings, is buzzing as a result of chemical reactions in every cell. In reality, these reactions are very slow and hence catalyzed by enzymes. Enzymes are nothing but specific types of proteins present in every living thing. Many of these natural enzymes can be extracted and they are capable of working *in vitro*. In the pharmaceutical industry, enzymes are usually used as drug targets, and hence play a key role in drug discovery. Pharmaceuticals will remain the largest and fastest growing market for enzymes, followed by the diagnostic and research/biotech segments. Currently, the US enzymes industry is \$2 billion, and demand for enzymes is expected to grow six percent annually through 2010. Ethanol production, recombinant human glycosidases, and animal feed phytase will also be amongst the fastest growing enzymes (Piribo 2006). Characterization of existing and new enzymes is a highly demanding as well as imperative process, and it is characterized by conducting enzyme kinetics experiments.



Essentially, an enzyme is characterized by its activity. Enzyme kinetics experiments are extremely repetitive, cumbersome, and incredibly slow. Extraction of enzymes from cell cultures is a very lengthy process, and economical use of enzymes would be a stringent requirement. Occasionally, a few enzymes are very rare and usage of smaller volumes is enforced on researchers conducting these experiments. However, conventional enzymatic reaction protocols require fair amounts of enzyme for conducting the experiments. Considering these drawbacks and limitations of conventional enzyme kinetics experiments, implementation on a microfluidic platform is of great consequence in today's fast moving and cost conscious industrial setting.

## **1.2 LAB-ON-A-CHIP (LOC)**

Lab-on-a-chip is basically a miniaturized device that manipulates tiny amounts of volumes in micro/nanometer scale channels and which also automates and integrates many biomaterials processing steps on a single chip (Daw and Finkelstein 2006; Whitesides 2006).

Typical advantages of LOC are:

- Lower consumption of sample and hence less wastage
- Reduction in the cost of conducting experiments
- Faster reaction due to improvement in diffusion, heating and cooling
- Better process control and hence better results
- Integration of innumerable steps could be possible on a single chip

Peculiar disadvantages of LOC include:

- Technology is still under research and development
- With current microfabrication techniques, mass production of LOC is difficult
- Precise geometrical control of channels and chambers is not very easy
- Many of the small scale phenomena are not very well studied and hence their behavior prediction and implementation on LOC is still a daunting task
- Detection of changes in the sample during the reaction could be slow and/or imprecise with conventional detection systems

### **1.3 HISTORY OF LAB-ON-A-CHIP**

In the 21<sup>st</sup> century, biology is witnessing unprecedented growth the way computers have witnessed in the last century. The aim of computers was to automate computations and that brought the revolution in our lives mainly in inanimate areas. However our animate life is still not totally explored and secured. For example we can fly and can do unimaginable activities by using PC and other machines, but still die due to cancer and other diseases. To cope with this, biologists are working hard in developing drugs and techniques to cure cancer and other diseases, delay aging and many more things in our animate life. However they are not having economical and very fast engineering tools to develop such drugs and techniques. Hence laboratory automation in biology and chemistry is the next revolution in engineering which is on its way. Figure 1.1 illustrates the comparison of automation of computer and automation in biological revolution. The current status of biological automation is in between the 1<sup>st</sup> and the 2<sup>nd</sup> stage and biologist would like to have tools equivalent to palmtop in future.

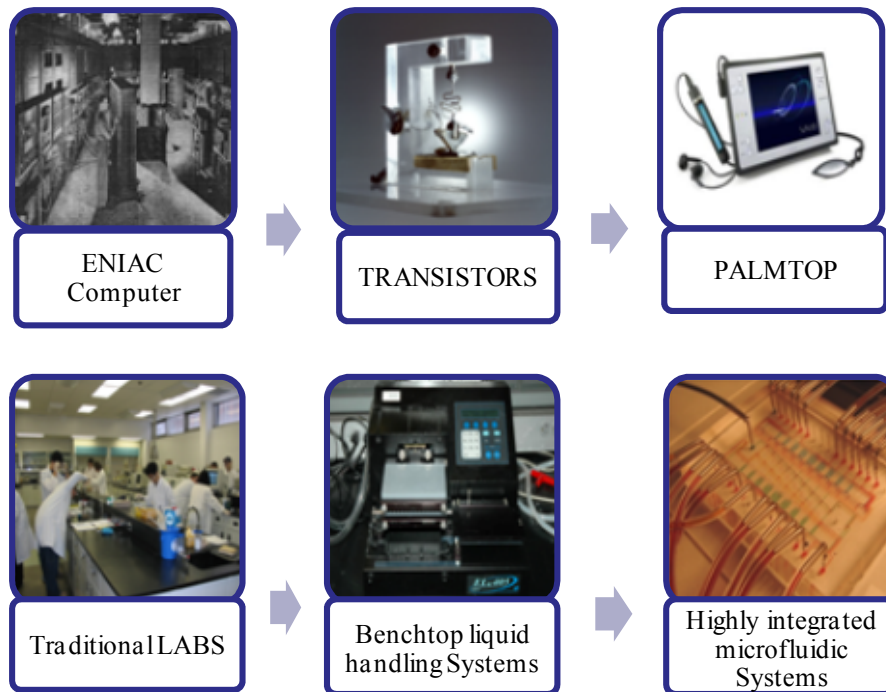


**Figure 1.1 :** Pictorial history of the developments in the area of microelectronics and Lab-on-a-chip.

*Source: All the pictures are adopted from the web.*

The amount of research carried out in the field of microfluidics has grown tremendously over the past 10 years, largely due to interest in the “lab on a chip” concept (Kamholz 2004). Microfluidic devices offer a different functionality compared to traditional macroscale devices. The most significant benefit derives from the notable reduction in the length scales. The result is an increase in surface area to volume ratio, making surface phenomena increasingly influential. This characteristic facilitates reduced sample requirements, improved heat transfer to and from the fluid, and faster processing time (Reyes, Iossifidis *et al.* 2002; Whitesides 2006),(Squires and Quake 2005; Whitesides 2006). The mechanics of fluid flow is affected by this reduction in length scale, as viscous forces become dominant over inertial forces (Nguyen and Wereley

2006). This relationship is quantified by the Reynolds number, a non-dimensional measure of the relative importance of advective and diffusive momentum transport, or in other words inertial and viscous effects.

The current research is one of the novel attempts to strive towards biological experimental palmtops. The ultimate goal of the project is to automate enzyme kinetics experiments, one of the fundamental and widely used experiments in biology. This revolutionary concept can be pictorially seen Figure 1.2 below

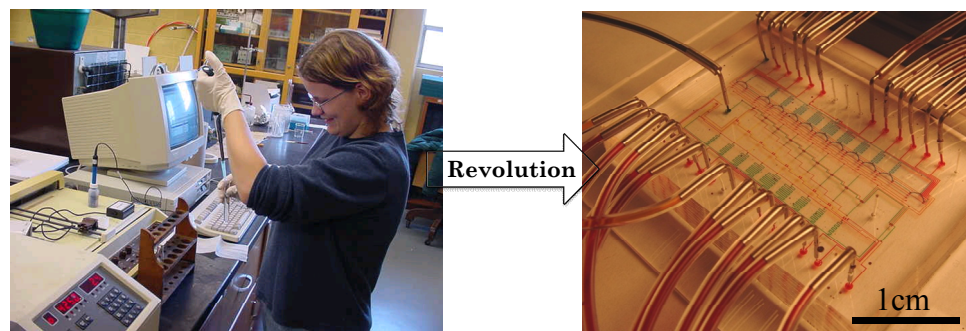


**Figure 1.2 :** Revolution from conventional enzyme kinetics experiment to protein kinetics chip  
**Source:** *Picture at the left is adopted from (Dettmer 2001-2004)*

#### 1.4 MULTILAYER SOFT LITHOGRAPHY (MSL)

The two most well-known methods for the production of microelectromechanical systems (MEMS) are bulk micromachining and surface micromachining. Bulk micromachining is a subtractive fabrication method whereby single-crystal silicon is lithographically patterned and then etched to form three-dimensional (3D) structures. Surface micromachining, in contrast, is an additive method where layers of semiconductor-type materials (polysilicon, metals, silicon oxide, silicon nitride, and so forth) are sequentially added and patterned to make 3D structures (Madou 1998).

Bulk and surface micromachining methods are limited by the materials used. The semiconductor-type materials typically used in bulk and surface micromachining are stiff materials with Young's modulus 107 GPa (see Table 1.1). As the forces generated by micromachined actuators are limited, the stiffness of the materials limits the minimum size of many devices. In addition, since multiple layers must be built up to make active devices, adhesion between layers is a problem of great practical concern. For bulk micromachining, wafer-bonding technique must be used to create multilayer structures. For surface micromachining, thermal stress between layers limits the total device thickness to about 20  $\mu\text{m}$ . Clean-room fabrication and careful control of process conditions are required to realize acceptable devices.

**Table 1.1** : Comparison of Young's moduli of PDMS and other common MEMS materials.

Material	Young's Modulus	Source
Silicon	107 GPa	(Madou 1998)
Silicon oxide	71 GPa	(Madou 1998)
Silicon nitride	100-200 GPa	(Madou 1998)
PDMS	750 kPa	(Unger, Chou <i>et al.</i> 2000)

An alternative microfabrication technique based on replication molding is quite popular in many areas of micro- and nanotechnology for device development. This technique is quite commonly known as soft lithography. Soft lithography (Xia and Whitesides 1998), was pioneered by Whitesides' group at Harvard University. Its advantages include the possibility for rapid prototyping, ease of fabrication without expensive equipment, and flexible process parameters. For a complete understanding of multilayer soft lithography, it is extremely important to understand the process of soft

lithography. Soft lithography is essentially the curing of a polymer on top of a negative mold structure. The process can be divided into two steps: negative mold fabrication and replica casting. Mold structures can be made by several different methods and are similar to the templates previously described for other replication methods. These methods include the micromachining of silicon (Madou 1998), LIGA (Hruby 2001), and the photolithographic patterning of photoresist (McDonald, Duffy *et al.* 2000). The mold type to be used is decided based on cost and production scale. More durable and better-defined molds are more expensive to make, but can withstand the harshness of large volume production and thus are more useful for industrial applications. Alternatively, inexpensive, quickly produced molds are ideal for most research and prototyping. Also, as polymer curing times are typically on the order of hours, soft lithography allows for very short device production times.

In the following sections, the principle of multilayer soft lithography is discussed. The multilayer soft lithography method is one of the most appropriate methods for devising monolithic elastomeric valves and mixers, which have a huge set of possible applications in the field of microfluidic devices, especially when used for implementing biotechnology protocols.

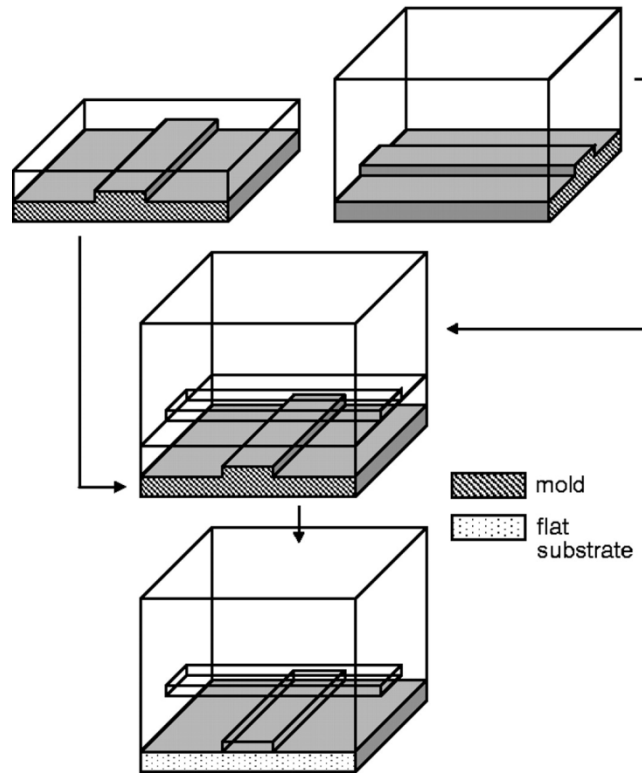


**Figure 1.2:** Principle of Multilayer Soft Lithography(MSL)  
**Source:** [(Unger, Chou *et al.* 2000)]

Unger *et al.* (2000) have developed a technique called ‘multilayer soft lithography’, which combines soft lithography with the ability to bond multiple patterned layers of elastomer together by varying the relative composition of a two-component silicone rubber between them. The simplicity of producing multilayers makes it possible to have multiple layers of microfluidics, a difficult task with conventional micromachining. Researchers have created test structures of up to seven patterned layers in this fashion, each  $\sim 40 \mu\text{m}$  in thickness. Because the layer assemblies are monolithic (i.e. all of the layers are composed of the same material), interlayer adhesion failures and thermal stress problems can be totally avoided.

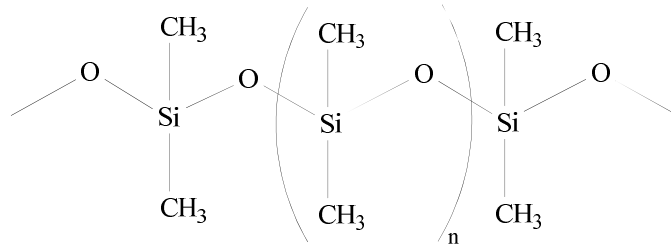
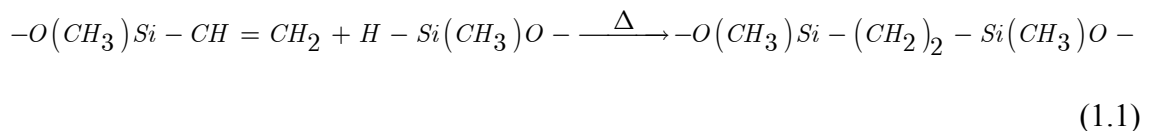


**Figure 1.3 :** Chemical structure of Silicone rubber or polydimethylsiloxane (PDMS)

The scheme behind multilayer soft lithography is shown in Figure 1.2. Two bonding layers are separately cast by using microfabricated molds. The elastomer used is a two-component addition-cure silicone rubber (GE RTV 615) [Figure 1.3]. RTV 615A contains a polydimethylsiloxane bearing vinyl groups and a platinum catalyst, whereas RTV 615B contains a cross-linker with silicon hydride (Si-H) groups which form covalent bonds with vinyl groups while heat curing as given in equation 1.1.. The bottom layer has an excess of one of the components (A), whereas the upper layer has an excess of the other (B). After separate curing of the layers, the upper layer is removed from its mold and placed on top of the lower layer, where it forms a hermetic seal.



Since each layer has an excess of one of the two components, reactive molecules remain at the interface between the layers. Finally, the excess curing causes the two layers to form an irreversible bonding. The strength of the interface matches the strength of the bulk elastomer. This process creates a monolithic three-dimensional structure composed



entirely of elastomer. Additional layers can be added by simply repeating the process. Each time the device is sealed on a layer of opposite ‘polarity’ (A versus B) and cured, another layer is added.

Subsequently, as the elastomer is a soft material with Young’s modulus  $\sim 750$  kPa (see Table 1.1), it may be subjected to large deflections with small actuation. Hence it could be most proficiently applied as the actuators (valves and pumps) for microfluidic systems.

## 1.5 MICROFLUIDICS

Microfluidics is a multidisciplinary field encompassing physics, chemistry, engineering and biotechnology that studies the behavior of fluids at the microscale and mesoscale, that is, fluids at volumes thousands of times smaller than a common droplet. More precisely, microfluidics is the science of designing, manufacturing, and formulating devices and processes that deal with volumes of fluid on the order of nanoliters or picoliters. The devices should also have dimensions varying from millimeters (mm) down to micrometers or even nanometers (Squires and Quake 2005; Nguyen and Wereley 2006; Whitesides 2006) [Figure 1.4]. In recent times, microfluidic systems have attracted diverse and well-known potential applications including flow cytometry (Fu, Chou *et al.* 2002), protein crystallization (Hansen, Skordalakes *et al.* 2002), DNA extraction (Hong, Studer *et al.* 2004), digital PCR amplification (Warren, Bryder *et al.* 2006), stem cell culture (Gomez-Sjoberg, Leyrat *et al.* 2007), and synthetic ecosystems consisting of *Escherichia coli* populations (Balagadde, Song *et al.* 2008).

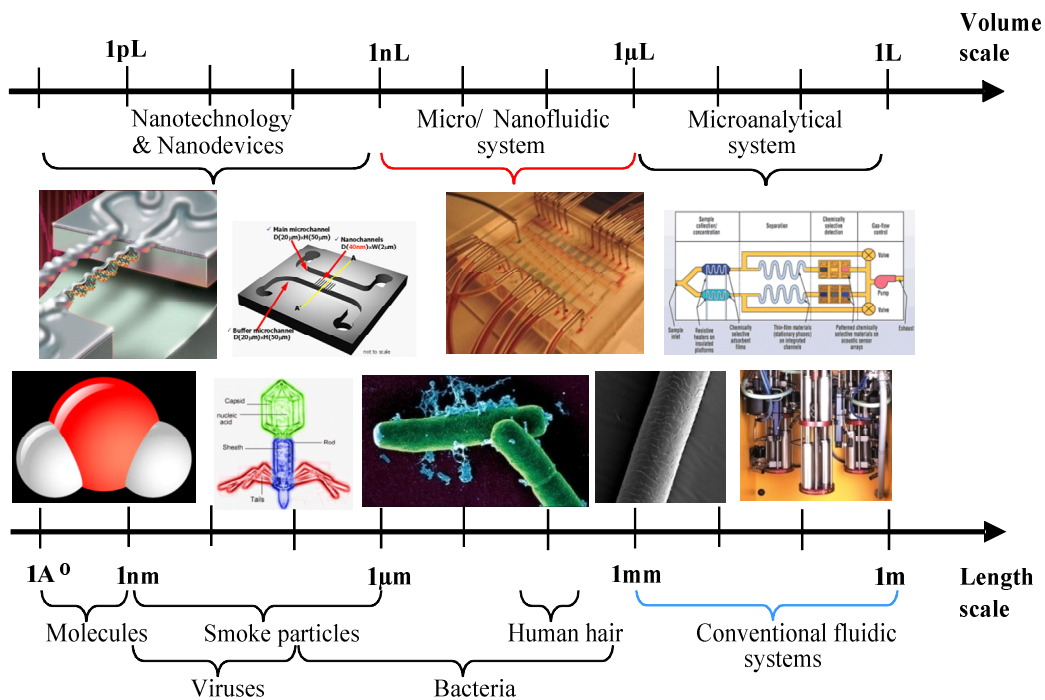


**Figure 1.4 :** Size characteristics of protein kinetics chip in relation with other objects.  
**Source:** All the pictures are adopted from the web.

## 1.6 MICROFLUIDIC PNEUMATIC VALVE

Since the microfluidic pneumatic valve is one of the key elements of the protein kinetics chip, it will be described in this section. In recent years, Quake and his group have pioneered the technique of fabricating microfluidic pneumatic valves in PDMS (Unger, Chou *et al.* 2000). Multilayer soft lithography (MSL) is used to create these monolithic elastomeric pneumatic microvalves by utilizing two layers in a cross-channel architecture. This is shown in Figure 1.5. Two types of valves can be constructed based on the relative position of the control layer, i.e., top or bottom. When the control channel is positioned as the upper channel, the membrane deflects downward when pressure is

applied to it. This configuration is called ‘push down geometry’. Devices with push down geometry may be peeled up, washed, and reused. In ‘push up geometry’, the control channel lies beneath the fluidic channel, and when pressure is applied to the control channel the membrane moves upwards and closes the fluidic channel. Push up geometry is useful when higher fluid back pressures are used. The schematic in Figure 1.5 shows how a push-up type of valve works.

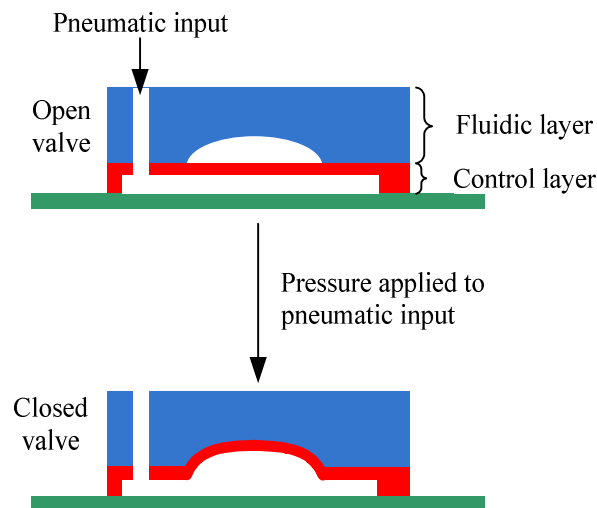


**Figure 1.5** : Schematic of valve closing for square and rounded channels.  
*After: [(Unger, Chou et al. 2000)]*

Typical channel dimensions, for both configurations, are 100  $\mu\text{m}$  wide and 10  $\mu\text{m}$  high, making the active area of the valve 100  $\mu\text{m}$  by 100  $\mu\text{m}$ . The polymer membrane between the channels is usually maintained to be relatively thin (between 10 to 30 $\mu\text{m}$ ). For reliable valve operations, push down geometry requires relatively thick membranes and more pressure as compared to push up geometry. Pneumatic actuation mechanisms allow microfluidic devices to be densely packed as the area of each valve is very small (100  $\mu\text{m}$  by 100  $\mu\text{m}$ ). The shape of the microchannel plays a very important role in the successful working of the valve. It has been observed that rectangular and trapezoidal-shaped

channels have problems with complete closure. However, a round shaped cross section with a parabolic profile closes completely. The membrane completely covers the round shape of the fluidic channel, hence closes it completely. An example of a closed channel is shown in Figure 1.6.

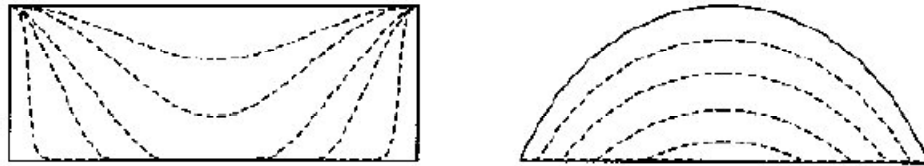


**Figure 1.6 :** Schematic of valve closing for square and rounded channels. The dotted lines designate the contour of the membrane in the rectangular (left) and rounded (right) channel as pressure is applied.

After: [(Unger, Chou *et al.* 2000)]

In the case of rectangular and trapezoidal-shaped channels, the membrane touches only at the center of the channel, resulting in incomplete closure. Hence to achieve a perfectly working microfluidic chip, fabrication of a rounded channel is a critical issue. This rounded shape can be attained by hard baking a photoresist above its glass transition temperature. At glass transition temperature the photoresist reflows and forms a rounded shape due to the balancing of surface tension. After the reflow, the height of the channel increases at the center, which keeps the volume of the photoresist constant.

In the last few years, exhaustive characterization and performance improvement of elastomeric microvalves has been conducted by many researchers (Unger, Chou *et al.* 2000; Studer, Hang *et al.* 2004; Kartalov, Scherer *et al.* 2007). The time constant for the on-off cycle is about a few milliseconds long. The working of the valve is stable and it can be used for over one million cycles. Thus, these valves can be used for precise and reliable control in microfluidic devices.

The on-off response times of a PDMS microvalve depends on the driving frequency, the switching time of the external pneumatic valve, the length and diameter of the control-line air channel, the shape and dimension of the valve itself, and the viscosity of the fluid flowing through the control and fluidic channels.

## **1.7 MICROFLUIDIC PNEUMATIC PERISTALTIC MIXER**

As discussed before, microfluidics holds the promise of integrating all the necessary functions onto a single chip. However, for the successful development of the lab-on-a-chip, there are many challenges to be dealt with. Rapid mixing of fluids flowing through microchannels is one of the most important issues. In microchannels, due to the small size, the Reynolds number is very small. For the laminar flow regime, mixing of fluids progresses mainly by diffusion, which happens very slowly. To solve this problem, various micromixers, such as chaotic flow micromixers, electrokinetic micromixers, peristaltic micromixers, etc., have been developed (Chou, Unger *et al.* 2001; Oddy, Santiago *et al.* 2001; Stroock, Dertinger *et al.* 2002; Nguyen and Wu 2005; Tai, Yang *et al.* 2006). For chaotic flow micromixers, microstructures placed on one side of microchannels generate flow circulation. The circulation leads to a dramatic increase in the interface between the fluids. Consequently, the mixing is improved. For electrokinetic micromixers, oscillating electroosmotic flows are used to enhance the mixing. When the electric field is applied to microchannels in the transverse direction and then oscillated, flow instability is initiated, which results in the improvement of mixing. For peristaltic

micromixers, multiple locations of part of a ring-shaped microchannel are deflected sequentially by using a minimum of three pneumatic controlled valves [Figure 1.7]. This peristaltic motion generates fluid flow in the microchannel and, in the course of the flow, the interface between the fluids is stretched very quickly, and this improves the mixing significantly. In a theoretical sense, the mixing is achieved by the process of peristalsis and Hagen-Poiseuille flow inside the microfluidic channel. In the last decades, to explore the potential of microfluidic systems, various approaches have been proposed and demonstrated (Haeberle and Zengerle 2007). Among them, microfluidic large scale integration (LSI) technology is recognized as one of the most promising microfluidic platforms. Since the peristaltic micromixer is one of the key elements of the protein kinetics chip, the present section is focused on the peristaltic micromixer.

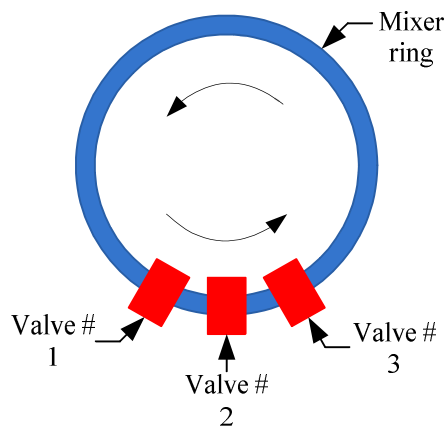


**Figure 1.7 :** Schematics of the working of a pneumatically operated peristaltic micromixer.

The peristaltic mixer is based on the multilayer soft lithography (MSL) process discussed before in Section 1.4. A minimum of three valves are considered necessary to break the spatial symmetry. The three valves are placed in sequence and the air pressure

for each valve is increased and released sequentially, as shown in Figure 1.8. Consequently, due to the sequential motion of the valves, fluid flow is generated in the fluid channel. When this peristaltic pump operates in a circular loop, an active micromixer is realized (Chou, Unger *et al.* 2001). Table 1.2 illustrates one possible sequence of valve operations for peristaltic fluidic motion inside the microchannel.

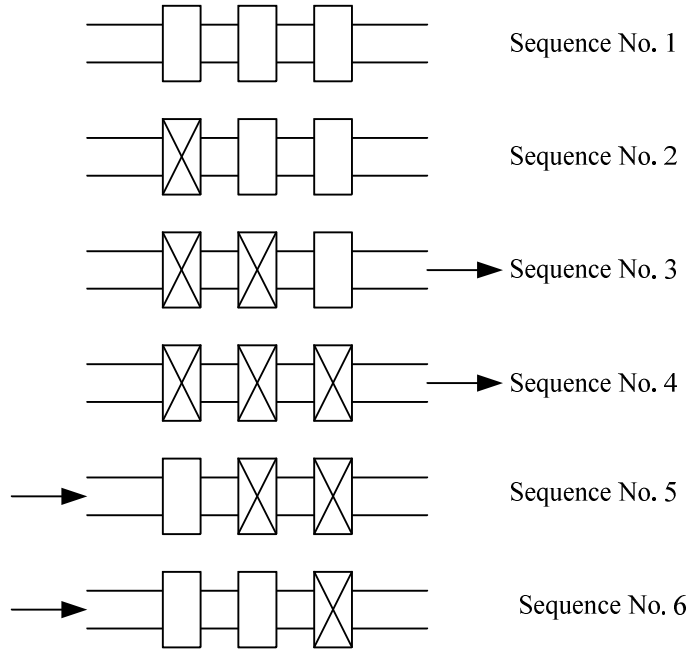


**Figure 1.8 :** Sequence of the valve operation during the working of a pneumatically operated peristaltic micromixer. The crossed rectangles represent closed position of the valve. The arrows indicate suction and the discharge cycle. The suction and the discharge volume is the volume under a valve.

**Table 1.2 :** Sequence of valve operation for peristaltic motion inside the microchannel (0 and 1 designate on and off state of the valve respectively).

Sequence No.	Valves on/off state( The order represents (Valve#1:Valve#2:Valve#3))
1.	0:0:0
2.	1:0:0
3.	1:1:0
4.	1:1:1
5.	0:1:1
6.	0:0:1

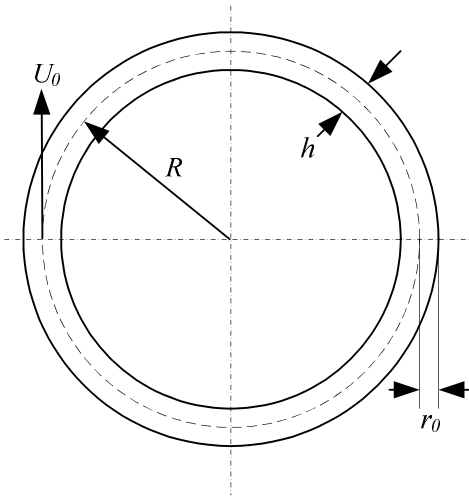


**Figure 1.9 :** Design parameters of pneumatically operated peristaltic micromixer.  
*After: [(Chou, Unger et al. 2001)]*

The design parameters of a pneumatically operated peristaltic micromixer are depicted in Figure 1.9. The angular velocity of the fluid inside the ring mixer (Chou, Unger *et al.* 2001) could be represented as

$$\omega_0 = \frac{U_0}{R} \left( 1 - \left( \frac{r}{r_0} \right)^2 \right) \quad (1.2)$$

where:

$U_0$  = maximum velocity at the center of the channel

$r_0$  = half of the width of the channel, and

$R$  = radius of the ring

The mixing time in the ring micromixer is directly proportional to the linear velocity of the fluid inside the channel.



## 1.8 ENZYME KINETICS

### 1.8.1 Enzymes

The early development of the concept of catalysis in the 19<sup>th</sup> century occurred simultaneously with the discovery of highly effective catalysts from biological sources. These were called ‘enzymes,’ and were later found to be proteins or protein-based molecules (Bugg 2004; Cornish-Bowden 2004). The central dogma of life is shown in Figure 1.10., where the formation of protein is depicted. Enzymes increase the rate of reaction in living cells without undergoing any permanent change in themselves (Palmer 1995). They are specific catalysts of vast range and utility. Their activity is governed by their structure and physical environment. In a typical situation, they increase the rate of reactions a million times.

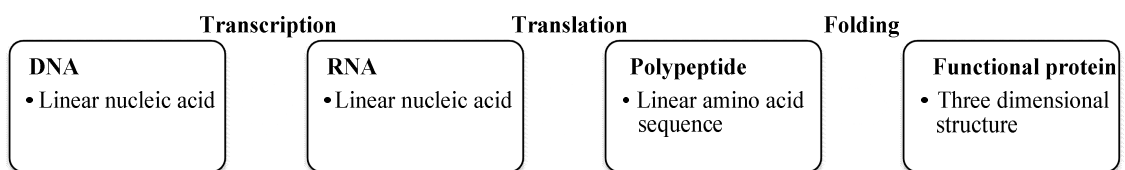


**Figure 1.10 :** Central dogma of life  
After: [(Palmer 1995)]

Enzymes are dynamic biomolecules, unlike DNA, and are responsible for many cellular activities. They efficiently and reliably serve as catalysts, genetic regulators, conductors, insulators, receptors, transducers, pumps, motors, stores, transporters, scaffolds, walls, toxins, antitoxins, and much more. They are also referred to as Nature’s nanomachines (Mantle 2001).

The amount of an enzyme present in any sample or taking part in a reaction is

hard to determine in absolute terms (e.g. grams). This is on account of its low purity and varying proportions or the possibility of its presence in an inactive or partially active state. Hence most commonly used parameters are the activity of the enzyme preparation and the activities of any contaminating enzymes. The enzyme activities are usually measured in terms of the activity unit (U), which is defined as the amount which will catalyze the transformation of 1  $\mu$ mole of the substrate per minute under standard conditions. An additional unit of enzyme activity has been recommended as the S.I. unit. This is the katal (kat), which is defined as the amount of enzyme which will catalyze the transformation of one mmole of substrate per second under specific conditions (1 katal =  $60 \times 10^6$  U) (Palmer 1995).

### 1.8.2 The mechanism of enzyme catalyzed reaction

The general form of the equation for a single-substrate enzyme catalyzed reaction can be written as follows:



where:

$E$  = enzyme

$S$  = substrate

$P$  = product

$E \cdot S$  = enzyme-substrate complex, and

$E \cdot P$  = enzyme-product complex

Based on the principles of thermodynamics and kinetics, to undergo any reaction, reactant molecules must contain sufficient energy to cross a potential energy barrier. This barrier is known as the activation energy. The lower the potential energy barrier for the reaction, the more reactants have sufficient energy and, hence, the faster the reaction will occur. The rate of reaction will be higher with a small activation barrier. All types of catalysts, including enzymes, have the typical characteristics of forming a transition state during reactions, and hence lowering the free energy required for the reaction. As a result, the rate of the catalyzed reaction becomes faster as compared to the uncatalysed reaction. Classically, the enzyme catalyzed reaction passes through the two transition states  $E \cdot S$  and  $E \cdot P$ , with standard Gibbs free energy of the activation barrier,  $\Delta G_{cat}$ , whereas the uncatalysed reaction goes through only one transition state with standard free energy of activation,  $\Delta G_{uncat}$  (Bugg 2004). Figure 1.11 shows the energetic diagram for an enzyme catalyzed reaction.

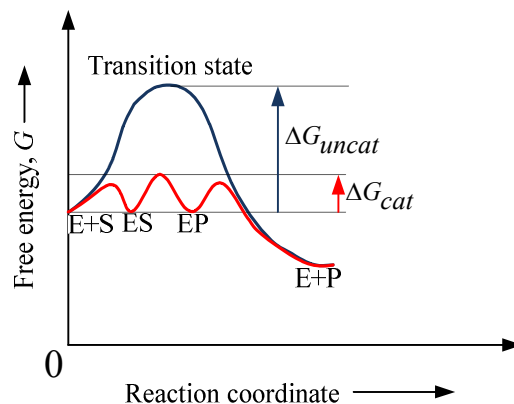


**Figure 1.11 :** Thermodynamical bioenergetics of enzyme catalyzed reaction.  
**After:** [(Palmer 1995; Cornish-Bowden 2004)]

The rate of enzyme catalyzed reaction is given by the well-known Michaelis-Menten equation:

$$v = \frac{V_{\max} [S]}{[S] + K_m} \quad (1.4)$$

### 1.8.3 Steady state kinetics

German biochemist Leonor Michaelis and Canadian medical scientist Maud Menten were the first scientists to characterize enzymes by utilizing the classical and highly popular Michaelis-Menten enzyme kinetics experiment. This experiment reported the quantitative measure of the kinetics of enzymes. Their study also showed that for many single-substrate enzyme catalyzed reactions, the relationship between initial velocity ( $v_0$ ) and substrate concentration  $[S]$  shows hyperbolic behavior, as given by the equation

$$v_0 = \frac{a[S]}{[S] + b} \quad (1.5)$$

where:

$[S]$  = substrate concentration, and

$a \& b$  = constants

In 1913, Michaelis and Menten proposed a kinetic model to elucidate their experimental results. They restricted the model to the initial period of reaction, where the

product concentration is negligible and reversible reaction from product to  $E \cdot S$  can be neglected. And the single substrate enzyme catalyzed reaction can be written



The rate of formation of  $E \cdot S$  at any time  $t$  (in the initial period when the enzyme product formation is negligible)

$$= k_1[E][S]$$

The rate of breakdown of  $E \cdot S$  at this time

$$= k_{-1}[E \cdot S] + k_2[E \cdot S]$$

Michaelis and Menten assumed that (Marangoni 2002),(Palmer 1995)

1. Equilibrium between enzyme, substrate, and the enzyme-substrate complex was achieved instantly and maintained throughout.
2. The conversion of product back to substrate is negligible, and
3. The concentration of substrate remains constant during the reaction.

Based on these steady-state assumptions,

$$k_1[E][S] = k_{-1}[E \cdot S] + k_2[E \cdot S] = [E \cdot S](k_{-1} + k_2)$$

$$\frac{[E \cdot S][S]}{[E \cdot S]} = \frac{k_{-1} + k_2}{k_1} = K_m$$

Where  $K_m$  is the constant

$$[E] = [E_0] - [E \cdot S]$$

where

$[E_0]$  = total concentration of enzyme,

$[E]$  = concentration of free enzyme, and

$[E \cdot S]$  = concentration of bound enzyme.

$$\frac{([E_0] - [E \cdot S])[S]}{[E \cdot S]} = K_m$$

$$K_m [E \cdot S] = ([E_0] - [E \cdot S])[S]$$

$$[E \cdot S] = \frac{[E_0][S]}{[S] + K_m}$$

Again, since  $v_0 = k_2 [E \cdot S]$

$$v_0 = \frac{k_2 [E_0][S]}{[S] + K_m} \quad (1.7)$$

In addition, when the substrate concentration is very high, the total enzyme gets converted into enzyme-substrate complex, and at that instant initial velocity, reaches a maximum. Therefore  $V_{\max} = k_2 [E_0]$

$$v_0 = \frac{V_{\max} [S]}{[S] + K_m} \quad (1.8)$$

The equation is similar to empirical relations proposed by Michaelis and Menten. It is referred to as the Michaelis-Menten equation, and  $K_m$  is known as the Michaelis constant. The plot of  $v_0$  against  $[S]$  gives a Michaelis-Menten plot and is shown in Figure 1.12.

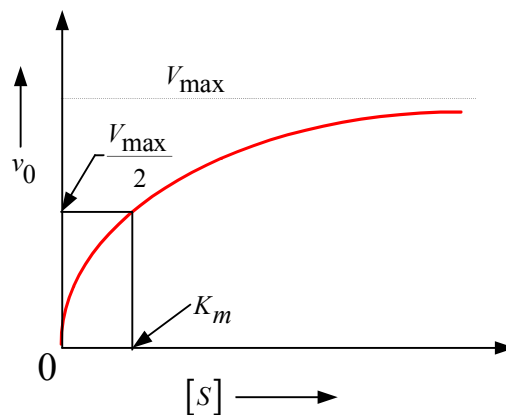


**Figure 1.12 :** Typical Michaelis-Menten plot for enzyme catalyzed reaction.  
*After: [(Palmer 1995)]*

While the Michaelis-Menten plot accurately represents the relationship between the initial velocity and the substrate concentration, its hyperbolic nature makes it difficult to extrapolate accurately the process for determining the values  $K_m$  and  $V_{\max}$ . To solve this problem, Hans Lineweaver and Dan Burk converted the hyperbolic relationship into a linear relationship. They basically inverted both sides of the Michaelis-Menten equation to yield the Lineweaver-Burk equation.

Hence the Lineweaver-Burk equation can be represented as

$$\frac{1}{v_0} = \frac{K_m}{V_{\max}} \frac{1}{[S]} + \frac{1}{V_{\max}} \quad (1.9)$$

The Lineweaver-Burk equation may be represented graphically by a double reciprocal plot as shown in Figure 1.13, also known as a Lineweaver-Burk graph.

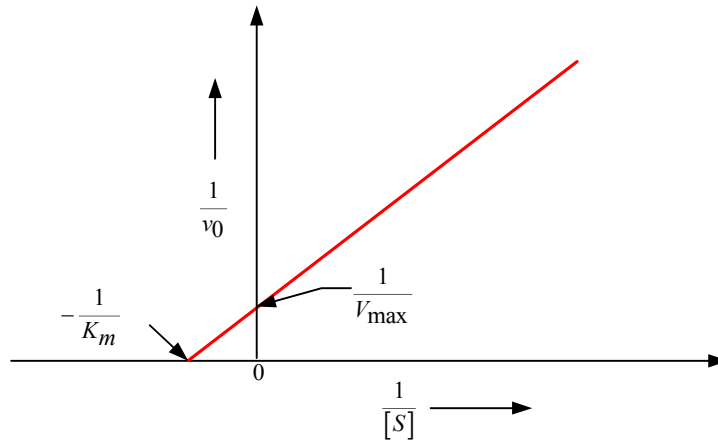


**Figure 1.13 :** Typical Lineweaver-Burk plot for enzyme catalyzed reaction  
**Source:** [(Palmer 1995)]

For conditions of constant temperature and pressure, the change in the Gibbs free energy,  $\Delta G$ , determines the direction in and the degree to which a reaction may occur. For an enzyme-catalyzed reaction, in which the substrate is converted into product in the presence of enzyme, the change in Gibb's free energy is given as follows:

$$\Delta G = \Delta G_0 + RT \ln \frac{[P]}{[S]} \quad (1.10)$$

where

$\Delta G_0$  = exponentially increasing distance between time points,

$R$  = universal gas constant, and

$T$  = temperature.

When  $\Delta G < 0$ , this process proceeds in the forward direction (substrate is converted into product); when  $\Delta G > 0$ , the reaction may possibly proceed backward (product is



converted into substrate); and when  $\Delta G = 0$ , there is no net progress and the reaction is at equilibrium. As a result, when  $[S]$  and  $[P]$  are at equilibrium,  $\Delta G = 0$ , and the equilibrium constant  $K_{eq}$  is

$$K_{eq} = \frac{[P]_{eq}}{[S]_{eq}} = \exp \left\{ -\frac{\Delta G_0}{RT} \right\} \quad (1.11)$$

## 1.9 ORGANIZATION OF THESIS

This thesis is divided into six chapters that clearly organize, illustrate, and describe the steps taken to meet the defined research objectives throughout the duration of this project. Immediately following this chapter, *Chapter 2: Literature Review* summarizes the body of knowledge pertaining to this study and synthesizes previous research efforts. The focus of the literature review is centered upon the microfluidic devices developed for conducting enzyme-catalyzed reactions. *Chapter 3: Protein Kinetics Chip: Development, Validation and Optimization* explains the process in the development of the Protein Kinetics Chip. Chapter 4 further explains the procedures followed for validating the working of the chip. *Chapter 4: Protein Kinetics Chip: Device testing with model enzyme* gives details about the selection of a model enzyme system for testing of the device. In the latter part of the chapter, the procedures for device testing, its data analysis, results and conclusion are given. Finally, *Chapter 5: Conclusions and Recommendations* provides concluding remarks regarding adequacy of the developed microfluidic platform, while benchmarking the developmental goals for further research that can be conducted to improve upon this research effort.

## **CHAPTER TWO**

### **LITERATURE REVIEW**

#### **1.1 INTRODUCTION**

The possible applications of microfluidics are increasing every year at a very rapid pace. A significant number of papers have been published related to enzymatic microchips in chemistry and biochemistry. Broadly, there are two types of devices central to the field of enzymatic microchips. In the first type, enzymes are immobilized on beads or walls of microfluidic channels. However, in the second type of devices, an enzyme reaction takes place inside a microfluidic channel (Urban, Goodall *et al.* 2006). The published research in the area of microfluidic devices used for enzyme kinetics can be categorized into three sections:

1. Microchannel and chamber based fluidic system
2. Droplet-based fluidic system
3. Microwell-based fluidic system

## 1.2 MICROCHANNEL AND CHAMBER BASED FLUIDIC SYSTEMS

Hadd *et al.* (1997) have explored a microchip device for conducting enzyme assays. The main focus of their project was to automate enzyme assay using a simple microfabricated channel network. A secondary focus of their research was to mix a precise amount of substrate, enzyme and inhibitor, in nanoliter-scale volume, by using the electrokinetic fluid transport phenomenon. In particular, reaction was carried out by varying precise concentration of substrate, enzyme and inhibitor and the kinetic information about the reaction was obtained by observing the fluorescence of the hydrolysis product. The microchip used for assaying the enzymatic reaction is shown in Figure 2.1. It was claimed that the reagent saving of four orders of magnitude is achieved when compared to a conventional enzyme assay.

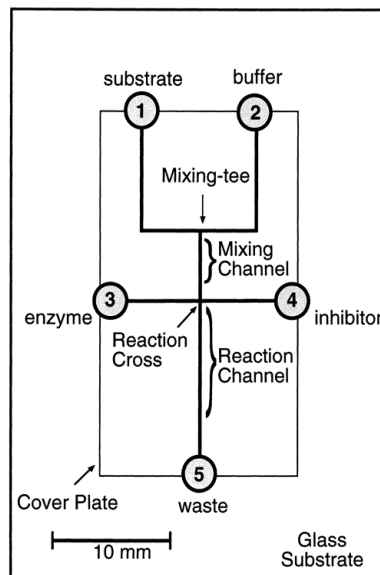


**Figure 2.1 :** Schematic of the enzyme analysis chip.  
**Source:** [(Hadd, Raymond *et al.* 1997)]

Seong *et al.* (1997) developed a microanalytical method for conducting enzyme kinetics using a continuous-flow microfluidic system. The device, used in this experiment, is shown in Figure 2.2. In this device, the enzyme was immobilized on microbeads and the substrate solution was passed through microbeads, packed into the microreactor, from left to right. The approximate volume of the microreactor was reported as 1 nL. The optical and fluorescence images were taken with a fluorescence microscope, and the fluorescence images were analyzed using precision digital imaging software. Two model enzymes were used to test the working of the microchip. In the first experiment, a horseradish peroxidase-catalyzed reaction between hydrogen peroxide and *N*-acetyl-3,7-dihydroxyphenoxazine (amplex red) was carried out to yield fluorescent resorufin. In the second experiment, the  $\beta$ -galactosidase enzyme reacts with non-fluorescent resorufin- $\beta$ -D-galactopyranoside substrate giving D-galactose and fluorescent resorufin. Experimental data were analyzed using the Lilly-Hornby equation and compared with result from conventional measurements based on the Michaelis-Menten equation. The device required *ca.* 10  $\mu$ L of substrate and  $10^9$  molecules of enzyme.

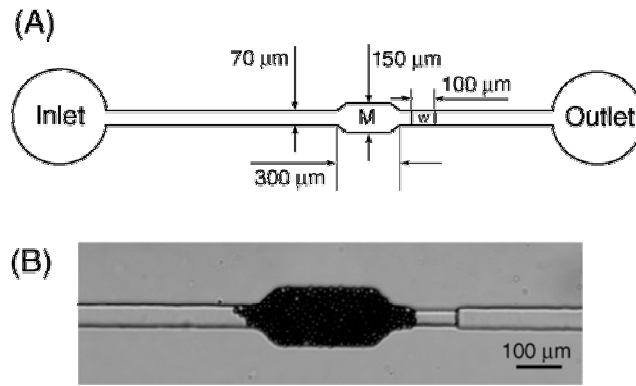


**Figure 2.2 :** (A) Schematic illustration of the microfluidic device used for analysis of enzyme kinetics. (B) Optical image of a microchamber after packing with microbeads.  
**Source:** [(Seong, Heo et al. 2003)]

Kang and Park (2005) reported a Polydimethylsiloxane- (PDMS) based microfluidic device compatible with microplate reader for optical detection. The device consists of 24 reaction chambers in a three-by-eight assay format. In each of the eight chambers, different concentrations of substrate were produced by passing two different streams of substrates through microfluidic channel networks. However, in each chamber, the concentration of enzyme is maintained constant. The microfluidic device is shown in Figure 2.3. In this research, alkaline phosphatase (ALP) enzyme and *p*-nitrophenyl phosphate (*p*-NPP) substrate was utilized for showing the capability of the device. The main feature of this device is its ability to allow simultaneous reaction in eight chambers.

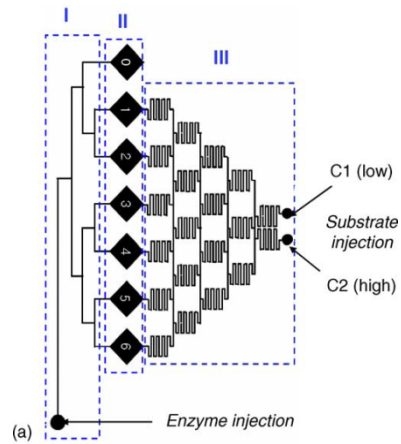


**Figure 2.3 :** (A) Schematic illustration of single enzyme assay in the microfluidic device.  
**Source:** [(Kang and Park 2005)]

### 1.3 DROPLET-BASED MICROFLUIDIC SYSTEMS

Due to diffusion-based reactions, the microchannel-based fluidic systems are limited in capturing the rapid kinetics. The limitation relates to type of mixing and dispersion. In microfluidics, typically the mixing is generated by diffusion or turbulence. The fast ( $k \approx 1000 \text{s}^{-1}$ ) and slow kinetics ( $k \approx 1 \text{s}^{-1}$ ) can be captured by using a *droplet-based* fluidic platform. The moving *droplet-based* platform employs chaotic advection, rather than the turbulence type of mixing [Song et al. 2003].

Song and Ismagoliv (2003) invented a microfluidic platform to address the problems of slow mixing and dispersion. They utilized the aqueous droplets to mix the reagents for rapid kinetic measurements. The droplets are generated and transported by pressure actuation. Figure 2.4 illustrates the principle of microfluidic system utilized for their measurement.

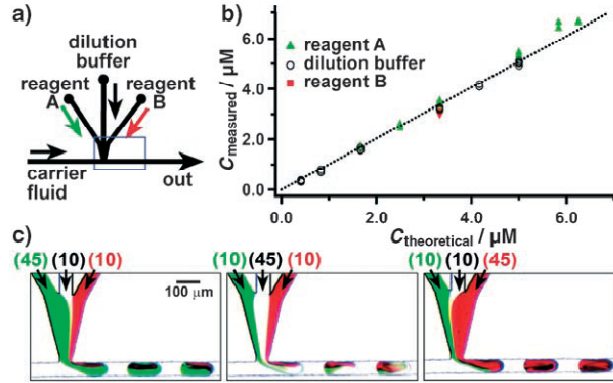


**Figure 2.4 :** Schematic illustration of mixing by chaotic advection inside the microfluidic channel.

Source: [(Song, Chen et al. 2006)]

They measured the rapid single turnover kinetics for ribonuclease A (RNase A) with millisecond resolution. The kinetic measurements were conducted by tracking the fluorescence of enzyme product down the microchannel. In order to capture first-order kinetics, it is necessary to scatter the measurement point at exponentially increasing distance.

The difference in the set of time measurement points can be given as

$$\Delta t(n) = \frac{(\Delta d_n)}{U} = \frac{(m_n \times l)}{U} \quad (2.2)$$

where

$\Delta t(n)$  = time interval between measurement points (n),

$\Delta d_n$  = exponentially increasing distance between time points,

$m$  = the factor of exponential increase

$n$  = index (from 1 to 8) numbering the time points, and

$l$  = unit length, (m).

The design of microfluidic channels for measuring first-order exponential kinetics is shown in Figure 2.5.

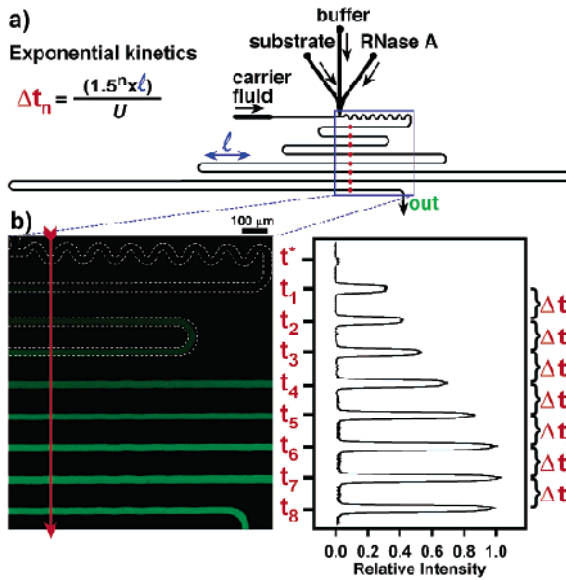


**Figure 2.5** : Design of microfluidic channels for measuring first-order enzyme kinetics.  
 Source: [(Song and Ismagilov 2003)]

Srinivasan *et al.* (2004) presented a *droplet-based* microfluidic chip for glucose detection. The chip uses discrete droplets manipulated by the electrowetting phenomenon powered by electrode potentials. The chip also integrates the optical detection systems and temperature systems, making it an integrated lab-on-a-chip platform. The platform is shown in Figure 2.6.



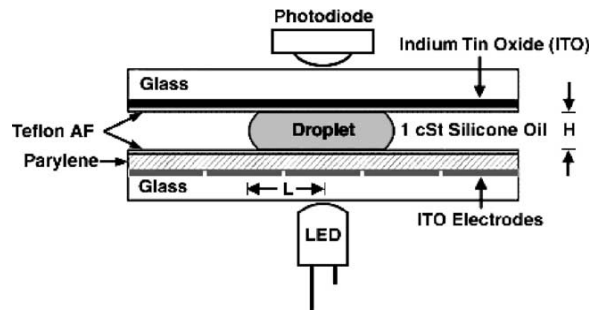


**Figure 2.6 :** Schematic of lab-on-a-chip for detecting glucose  
**Source:** [(Srinivasan, Pamula *et al.* 2004)]

#### 1.4 MICROWELL-BASED FLUIDIC SYSTEMS

Even after much research into microfluidics and lab-on-a-chip, high-throughput and parallel processing, devices matching the throughput of a conventional microarray are still rare. The reason for this deficiency could be attributed to, much emphasis on reduced sample consumption, low-cost devices, high-speed operation and detection, extreme automation and integration. To circumvent the above mentioned limitations of lab-on-a-chip devices, Young *et al.* (2003) introduced a silicon-etched nanoliter-scale well device. The key features of the device are nanoliter-scale sample consumption, automation for sample handling, throughput comparable to the microtiter plates, and highly automated real-time detection systems. The device can be seen in Figure 2.7. The system consists of 25 nano-liter scale wells arranged in 5x5 array formats. Figure 2.7 (a) shows the device at the backdrop of 96-well a microtiter plate. The nozzle-based electro spray mechanism is shown in Figure 2.7 (b). The electro spray has the capacity to deliver 240 pL of sample into each well. It is operated by an external fluidic handling system. The optical detection system and its electronics, in the form of an optical filter and photo diode, are positioned underneath the device.

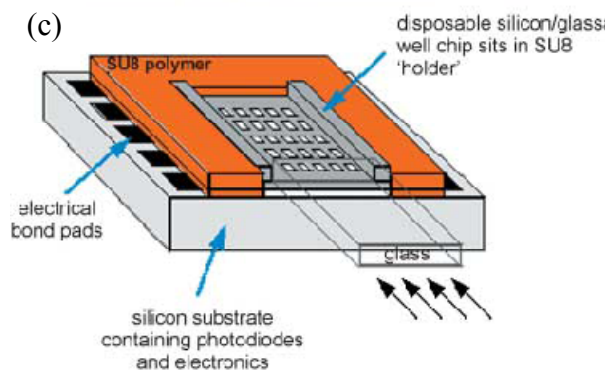
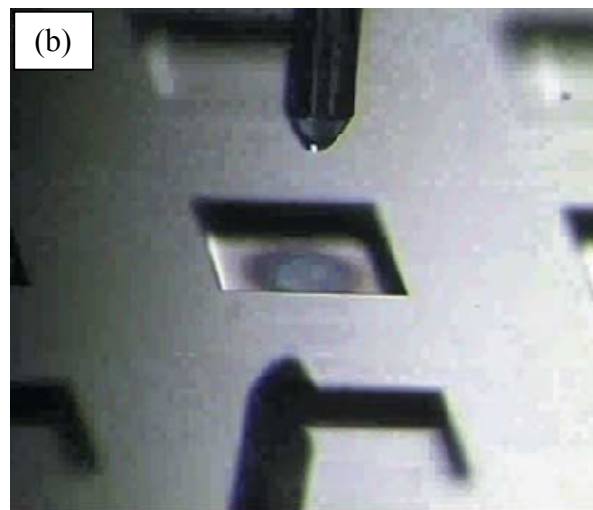
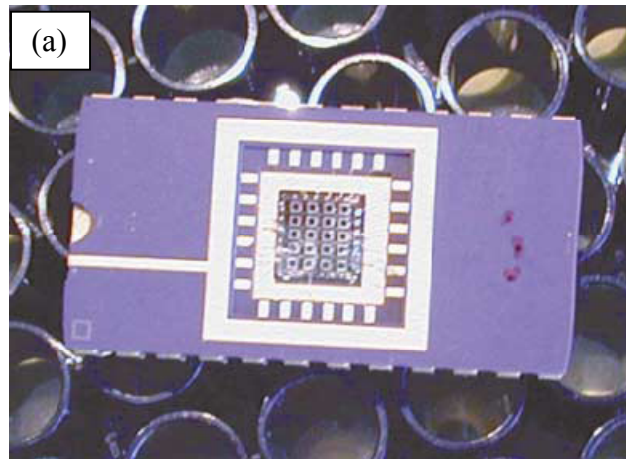


**Figure 2.7 :** (a) Picture of lab-on-a-chip having 5x5 array nano-liter scale wells etched in Si substrate. (b) Electro-spray nozzle system dispensing a nano-liter sample. (c) Schematic representation of working of the device.  
 Source: [(Young, Moerman et al. 2003)]

## 1.5 RESEARCH OBJECTIVES

The focus of this research is to develop a microfluidic platform for the rapid evaluation of kinetic parameters in an enzymatic reaction. The aim is to build and test a rectangular polymer-based chip allowing the simultaneous detection estimate of eleven reactions, including one positive and one negative control, in which a substrate gradient is generated using different volumes of substrate and dilution buffer, while the concentration of enzyme is kept constant by holding its volume constant. The specific goals of the research are as follows:

1. Design a microfluidic chip:
  - the chip is designed using AutoCAD<sup>®</sup> software,
  - the fundamental aim of the chip design: ability to process nano-liter scale enzyme, substrate and dilution buffer in a highly parallel manner for conducting multiple enzyme reactions simultaneously.
2. Fabrication of silicon mold to use as molds for chip fabrication.
3. Fabrication of polydimethylsiloxane- (PDMS) based microfluidic chip using the Multilayer Soft Lithography (MSL) technique.
4. Development of LabVIEW based program in order to control valves and mixers for the operation of the chip

5. Validation of the working of the entire chip operation by using food dye with various colors as enzyme, substrate and dilution buffer.
6. Investigation of model enzyme system in order to demonstrate the working of the developed microfluidic platform

**CHAPTER THREE**  
**PROTEIN KINETIC CHIP:**  
**DEVICE DEVELOPMENT, AND VALIDATION,**

**3.1 INTRODUCTION**

A protein kinetics chip is a complicated microfluidic platform built upon many tools and concepts. The major tools involved in the development of a protein kinetic chip include the following: computer-aided drafting (CAD), microfabrication and soft lithography. It is a computer-controlled platform capable of automatically dispensing, metering, mixing, washing and cleaning. The purpose of this chapter is to describe the development cycle and device validation of the protein kinetics chip. Figure 3.1 depicts the steps in the development of the protein kinetics chip.

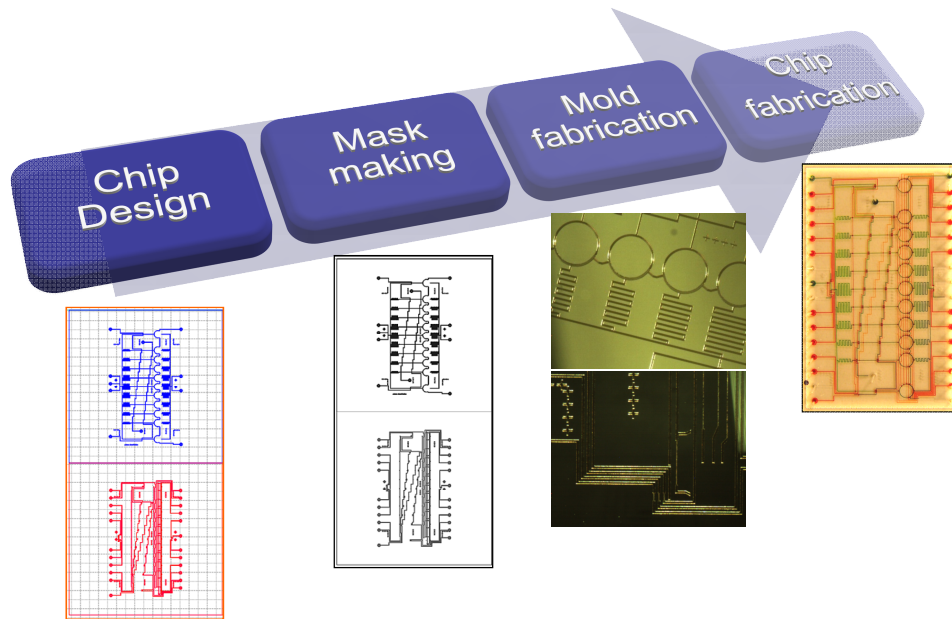


**Figure 3.1 :** Summary of process followed during development of protein kinetics chip.

### 3.2 DEVICE DESIGN

The focus of this section is to describe different design versions of the protein kinetics chip for the rapid evaluation of kinetic parameters of an enzymatic reaction. To design the chip, AutoCAD<sup>®</sup> software (Autodesk<sup>®</sup> Inc.) was utilized exhaustively. The designs prepared with the AutoCAD<sup>®</sup> software (Autodesk<sup>®</sup> Inc.) were sent for mask printing on a transparent film at 20000dpi (CAD/Art Services, Inc.).

#### 3.2.1 Benchmark design scheme

The preliminary design scheme of the protein kinetics chip is based on a DNA extraction chip published by Hong *et al.* (Hong, Studer *et al.* 2004). In the preliminary design scheme, it was decided to start with the following broad goals:

- The chip should automate the process of metering, concentration gradient

generation, mixing and optical detection.

- In addition, as the preliminary design attempt the chip could be designed with inclusion of eleven numbers of parallel processors, with one negative and one positive control, it will have the capacity to conduct multiple processes simultaneously.
- It should have the operational scheme as summarized in Table 3.1.

The microfluidic systems, named ‘protein kinetics chip,’ could also be used for biological and chemical material processing which require parallel processing. However, the emphasis is placed on obtaining kinetic parameters for an enzymatic reaction on a chip.

**Table 3.1** : Summary of operational scheme of protein kinetics chip.

<b>Operation</b>	<b>Figure</b>
Dilution buffer and substrate is supplied to the processor	3.2a
Dilution buffer and substrate is pushed into the mixer	3.2b
Enzyme is supplied to the mixer ring	3.2c
Mixing is started inside the ring mixers by operating peristaltic valves	3.2d
Wash buffer is supplied for cleaning the chip	3.2e
Air is supplied for drying the chip	3.2f

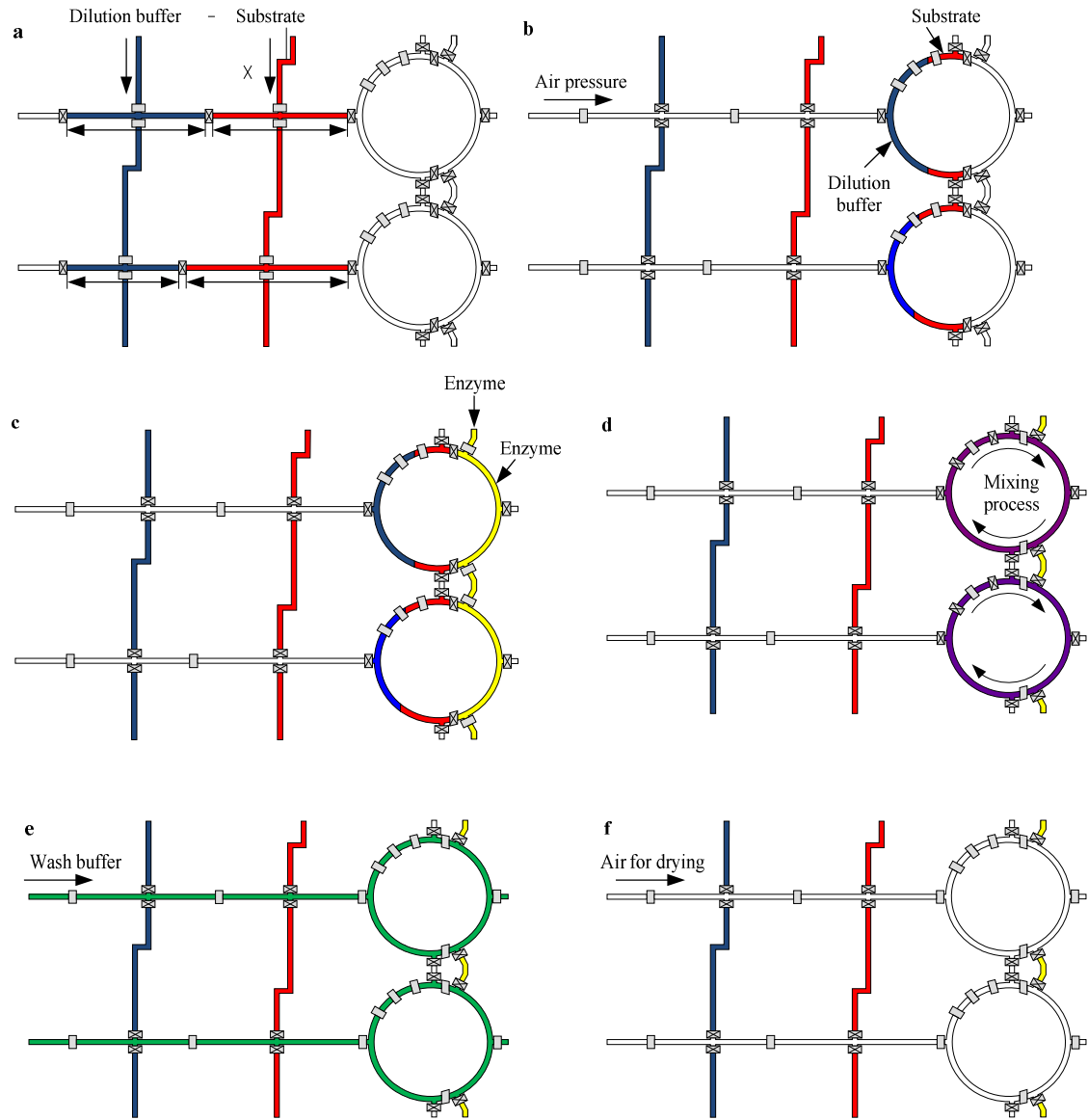


**Figure 3.2 :** Schematics of operational scheme of protein kinetics chip.

### 3.2.2 Protein kinetics chip design Version. 1

All the valves were designed with valve dimensions of 100  $\mu\text{m}$  by 100  $\mu\text{m}$ . The fluidic and control channel width is also uniformly maintained at 100  $\mu\text{m}$  throughout the chip. However, during the testing of the chip with this design, the chip showed



inconsistent mixing in the rings; hence, the design was changed. The design of version.1 is shown in Figure. 3.3a. The version .2 of the design is discussed in the next section.

### **3.2.3 Protein kinetics chip design Version. 2**

In this design, the valve width was modified to 150  $\mu\text{m}$  for faster and reliable operation. The control channel width was maintained at 50  $\mu\text{m}$  for faster valve operation and reduced hydraulic resistance. However, the fluidic channel was also maintained at 100  $\mu\text{m}$ . And, as the mixing valve width increased, flow rate through the mixing loop increased, and this resulted in reliable mixing. Figure.3.3b illustrates the design of version.2 of protein kinetic chip. In the course of operation of the version.2 of the chip, it was observed that the chip worked successfully throughout the entire operation except during cleaning.

### **3.2.4 Protein kinetics chip design Version. 3**

Figure 3.3c demonstrates the design of ver.3 of protein kinetic chip. In this design, the only modification was to provide additional inlet and exit channels for cleaning operation. The modification proved to be successful for accelerated cleaning of the chip.

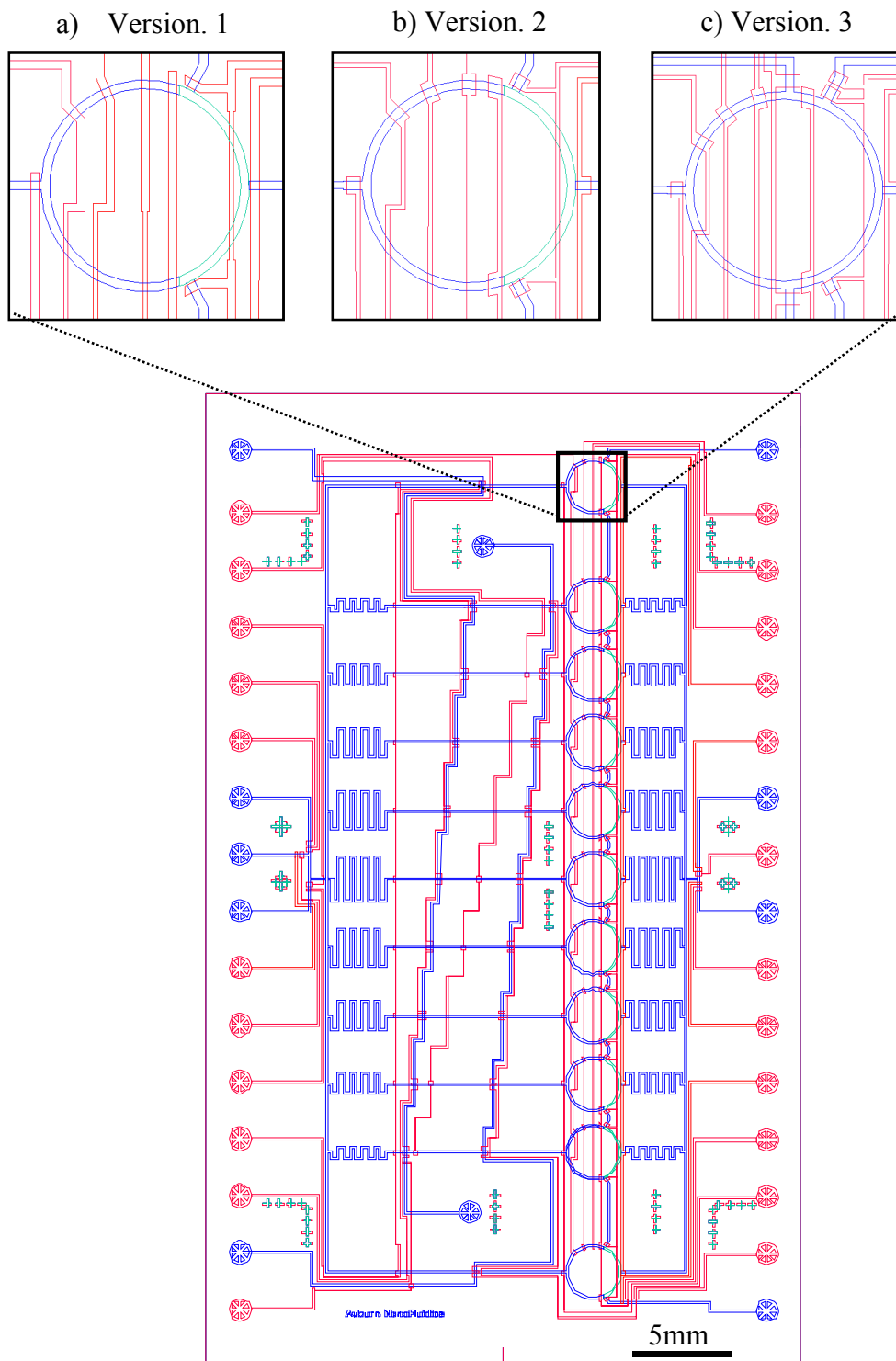


**Figure 3.3** : Design versions of protein kinetics chip.

### **3.3 MOLD FABRICATION**

The molds were fabricated at the Alabama Microelectronics Science and Technology Center (AMSTC) at Auburn University. Two separate molds were fabricated for the fluidic and control layers. However, similar fabrication processes were adopted for them, except for a few changes in process parameters. The fabrication process is schematically depicted in Figure 3.4. The quality of molds is highly dependent on the processing parameters involved in making them. The processing parameters are, to some extent, equipment-specific. The optimization of processing parameters to achieve the required geometrical parameters is an iterative process. To quantify the iterative process, the quantum of work included fabrication and testing of more than 50 molds and 50 PDMS chips. The mold fabrication procedure using thick photoresist structures is detailed in this section.

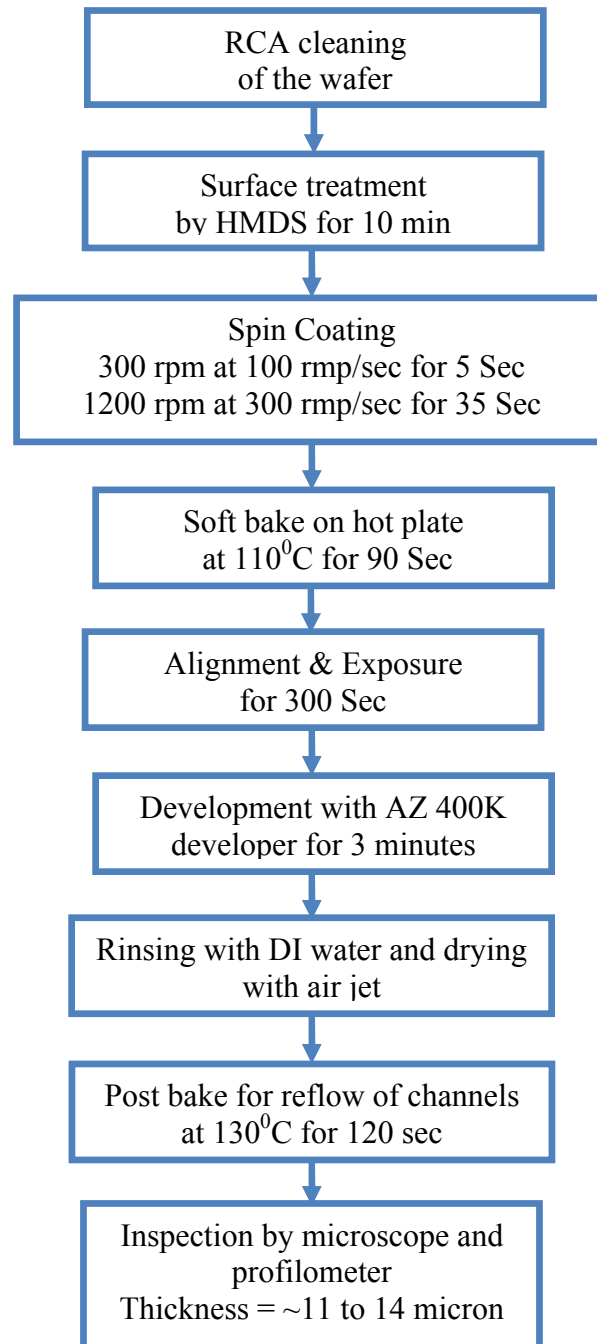


**Figure 3.4 :** Process flow diagram showing mold fabrication process during development of protein kinetics chip

The silicon microfabrication technique is utilized in the fabrication of molds. To ensure a high-quality photoresist coating, the silicon wafer surface must be properly cleaned as contaminants readily cause defects in the photoresist layer. To accomplish this clean wafer surface, a three-step RCA cleaning procedure was adapted. The RCA cleaning procedure was followed sequentially and is given here (Kern 1993),(Kern and Vossen 1978):

1. **Organic clean:** Used for removing insoluble organic residues with a 5:1:1 of  $\text{H}_2\text{O}:\text{H}_2\text{O}_2:\text{NH}_4\text{OH}$  solution.
2. **Oxide strip:** Used for removing a thin silicon dioxide layer at which metallic contaminants may accumulate as a result of using a diluted 50:1 of  $\text{H}_2\text{O}:\text{HF}$  solution.
3. **Ionic clean:** Used for removing ionic and heavy metal atomic contaminants using a solution of 6:1:1 of  $\text{H}_2\text{O}:\text{H}_2\text{O}_2:\text{HCl}$ .

Just before use, the RCA-cleaned wafer was dehydration-baked at  $150^\circ\text{C}$  for 10 min to evaporate any traces of water on the substrate. The silicon wafer was exposed to hexamethyldisilazane (HMDS) vapor for 10 min. HMDS promotes the adhesion of photoresist to the wafer. A variety of photoresist can be employed for mold fabrication. A variety of AZ photoresists are available, with typical patterned thicknesses ranging from  $2\ \mu\text{m}$  to  $20\ \mu\text{m}$  due to the variation in photoresist viscosity. AZP4620, a common thick, positive photoresist was used exclusively for both fluidic and control layer molds due to the desired height of 10 to  $20\ \mu\text{m}$ . A thin AZP4620 photoresist layer was formed

on a plane substrate by spin-coating. The thickness of the photoresist layer depends exclusively on the final rotational speed during spin-coating and the viscosity of the photoresist. An initial ramping stage from zero to 1000 rpm at an acceleration of 100 rpm/s serves to spread the photoresist and cover the complete substrate. Spinning speed was then accelerated at a rate of 300 rpm/s to the final speed and held for a total of 32 sec. Approximate correlations between spinning speed and the resulting photoresist thickness for AZ photoresists are provided by the supplier [MicroChem®]. However, knowledge of the exact dimensions of microfluidic channels is critically important for experimentation in which channel height is a critical parameter. The actual width is highly dependent on the exact processing parameters and composition of the photoresist. In order to better correlate the resulting channel height with spin speed, direct measurements of AZ photoresist layers were obtained. Near the edge of the substrate, photoresist thickness increases due to the well-known edge bead effect, a limitation of the spin-coating process (Lin, Lee *et al.* 2002). Excluding the near-edge bead where a non-planar surface was expected, the standard deviation in thickness measurements across a single coated slide typically ranged from 1  $\mu\text{m}$  to 5  $\mu\text{m}$ . However, in ideal cases photoresist layers self-planarize during the spin-coating and baking steps, creating a consistent height across the substrate. Fluctuations beyond 5  $\mu\text{m}$  in height across a single sample suggest the presence of defects due to improper processing or inconsistent surface of the base substrate.

Following the spin coating, photoresist layers are soft-baked to evaporate their solvent content and condense the photoresist film. Soft-bake temperatures and times for

the soft-baking process were provided by the supplier and proved appropriate. A soft bake at 110°C for 95 sec was sufficient for the evaporation and condensation process. One very important observation was the necessity of using a spirit-leveled hot plate to attain a totally flat photoresist surface of consistent height. During the soft bake process, photoresist layers are highly susceptible to contamination from airborne particulates. Hence, extra care was taken to avoid the settling of such particulates.

One of the very important steps of the mold fabrication process is exposing the photoresist through the photomask. Exposure to near-UV light of wavelengths between 350 nm and 400 nm locally generates acid which initiates photoresist cross-linking (Madou 1998). Insufficient exposure doses are unable to adequately initiate polymerization throughout the thickness of the photoresist, and transferred patterns are not strong enough to resist slight dissolution during the development stage. Detachment from the substrate surface can occur in cases of extreme underexposure. An upper limit to the exposure dose also exists. Over-exposing results in the creation of shadows, which are nothing but finite areas of partially exposed photoresist around the desired features due to a combination of Fresnel diffraction at the edge of opaque sections, refraction at the air-photoresist interface, and reflection from the base substrate. Improvements in the conformity of photoresist patterns to the photomask design can be attained by determining an optimal exposure dose, which is dependent on the photoresist thickness. The molds were exposed under UV light on a mask aligner (350 W and 2 mW/cm<sup>2</sup>) for 300 sec.

The molds were then developed in AZ 400k developer for 5 minutes with slight agitation of the photoresist. The time required to completely remove unexposed photoresist is dependent on the photoresist thickness, strength of agitation, feature size of the exposed pattern, and repeated use of the developer solution. While it is possible to determine an optimal development time for a given photoresist structure, this would be unique for the combination of the above mentioned parameters. Developing can be visually inspected to approximate when the process is complete.

### **3.4 CHIP FABRICATION**

All the protein kinetics microfluidic chips were fabricated by multilayer soft lithography (MSL) with the silicone elastomer polydimethylsiloxane (PDMS), General Electric), by use of photoresist- patterned mold. Each device employs pushup valve geometry and is a three-layer elastomeric structure bonded to a 3'' by 2'' clean glass slides. PDMS is commonly used, due to its many favorable characteristics including chemical stability, high reproduction fidelity, minimal cost, optical transparency (down to 280 nm), and ease of sealing. The procedure for chip fabrication using Polydimethylsiloxane is detailed in this section. Furthermore, the chip fabrication process is schematically summarized in Figure 3.5.



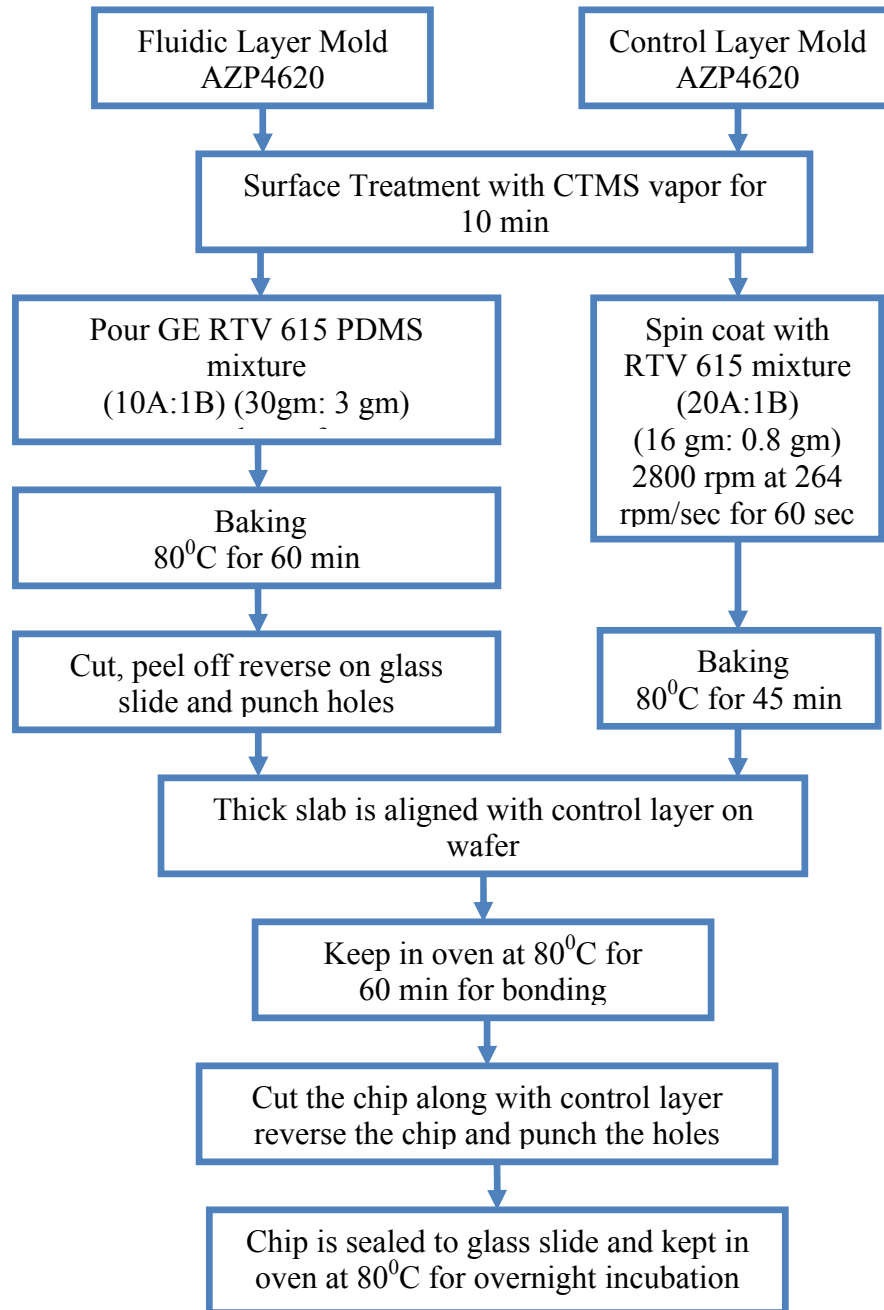


**Figure 3.5 :** Flow diagram showing chip fabrication process during development of protein kinetics chip.

For fluidic thick layer, PDMS was prepared by mixing the base and curing agent at a 10:1(30 g: 3 g) weight ratio. And, for the control layer, PDMS was prepared by mixing the base and curing agent in a ratio of 20:1 (12g: 0.6g). The mixed prepolymers were degassed under vacuum for approximately 2 hours or until all air bubbles were removed from the bulk polymer. The polymer was then poured over the mold structure in a manually prepared aluminum well prepared around the mold structure, and the poured PDMS was cured at 80°C for 60 min. The other liquid PDMS mixture (20:1) was spin-coated onto the control mold (2,800 rpm for 60 sec), and the coated control mold was kept on the flat surface for 30 min. in order to obtain a uniform elastomer membrane thickness on top of the control structure. The mold was then baked at 80°C for 45 min. Following baking, the partially cured fluidic layer was peeled from its mold. The peeled layer was transferred to a glass slide in an inverted position, and 20-gauge diameter flow channel access holes were punched into the chip under the microscope. Then, by appropriate use of alignment marks at both fluidic and control layers, they were aligned under the stereomicroscope. The assembly of aligned unbonded layers was performed in the oven at 80°C for 60 min for achieving irreversible bonding. For high-pressure leak-proof sealing of the chip on the glass slide, the third layer was fabricated by spinning liquid PDMS (20 parts A:1 part B) onto a clean glass slide (2,000 rpm for 60 s.). This was followed by baking at 80°C for 30 min. Once the bonding was completed for the two-layer chip, it was peeled from the control mold. The peeled-off chip was transferred to glass slide in an inverted position and 20-gauge diameter control channel access holes

punched into the chip under the microscope. Finally the two-layer chip was placed onto the third partially cured PDMS layer. The three-layer chip was then baked at 80°C for 18 hr. After the completion of 18 hrs incubation, the chip was ready for subsequent experimentation. Figure 3.6 shows the dye-filled chip.

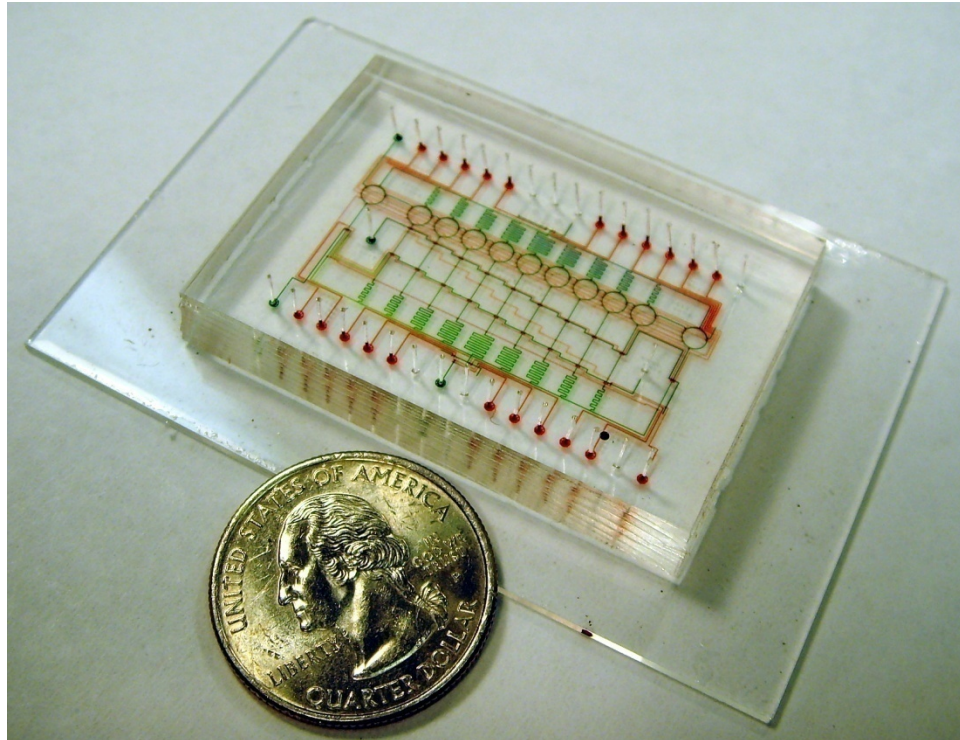


**Figure 3.6 :** Dye-filled protein kinetics chip with US quarter coin for size comparison

Membrane thickness of the control layer plays very important role in the smooth and reliable working on valve. Hence it is very important to measure the membrane thickness, control channel height and fluidic channel height right after fabrication of the chip. Figure 3.7 shows the membrane thickness along with the control channel height.

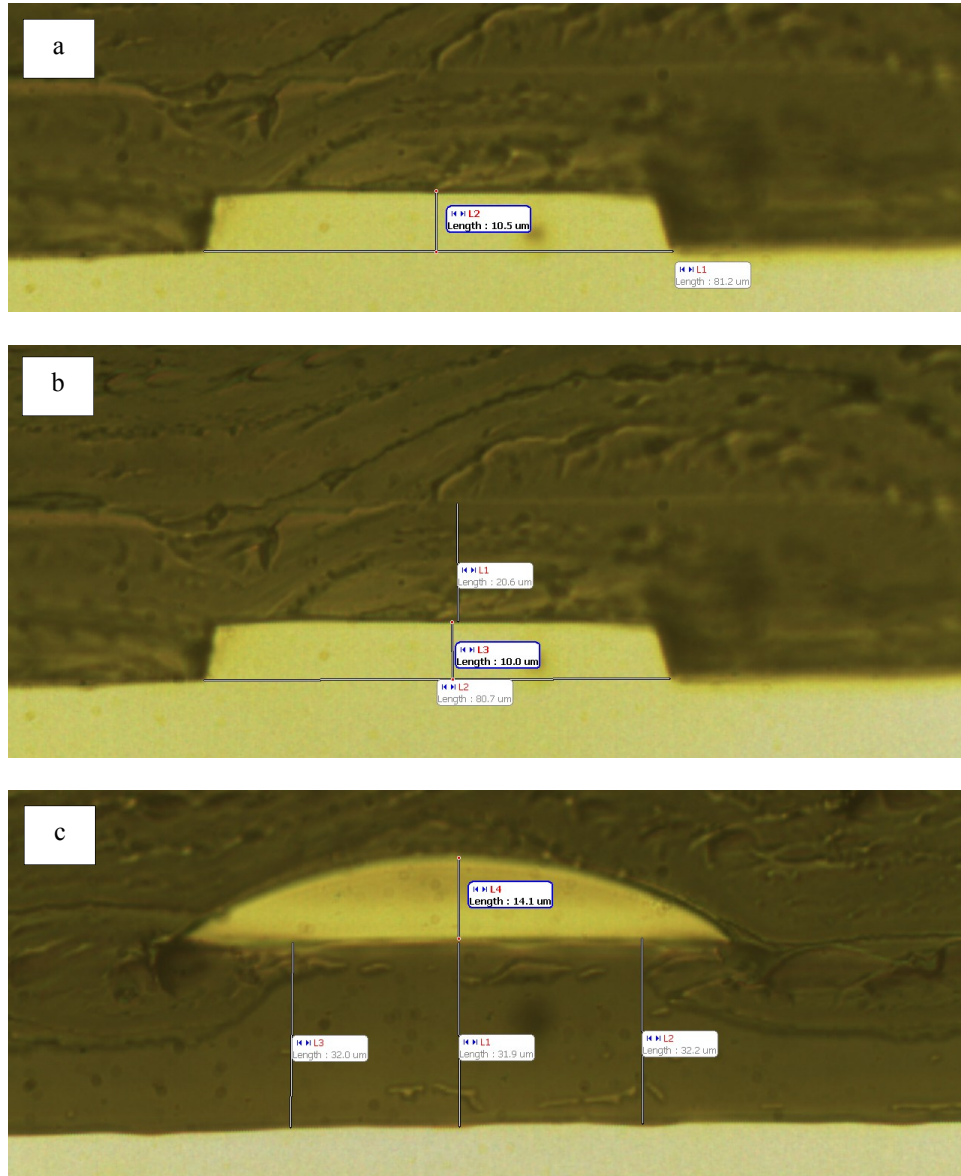


**Figure 3.7 :** Cut-section of the protein kinetics chip for the measurement of (a)control channel height;(b)membrane thickness and (c)fluidic channel height

### 3.5 DEVELOPEMENT OF LabVIEW® CONTROL PROGRAM

The pneumatic pressure controls solenoid pumps used for operating on-chip valves. In turn, the valves were controlled through a LABVIEW® software-based program developed for the proper functioning of the protein kinetics chip. For uninterrupted control of the chip, two separate programs were developed. The first program was utilized for control of individual valves, while the other was intended for control of valves required for operation of the ring mixer. Pictures of the front panel of programs used for this research are shown in Figure 3.8. For the sake of clarity, the block diagrams of valve control and mixer control are shown in Figure 3.9(a) and 3.9(b), respectively. This LABVIEW® code was used to operate multiple valves. The program was developed by considering the demands of future projects, so the number of valves could be extended according to experimental requirements.

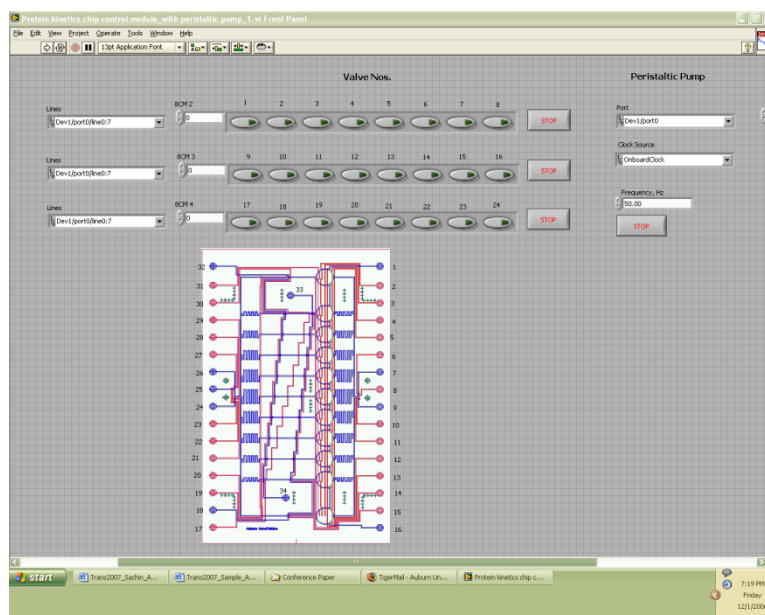


**Figure 3.8 :** GUI of LabVIEW® program utilized for operating the protein kinetics chip

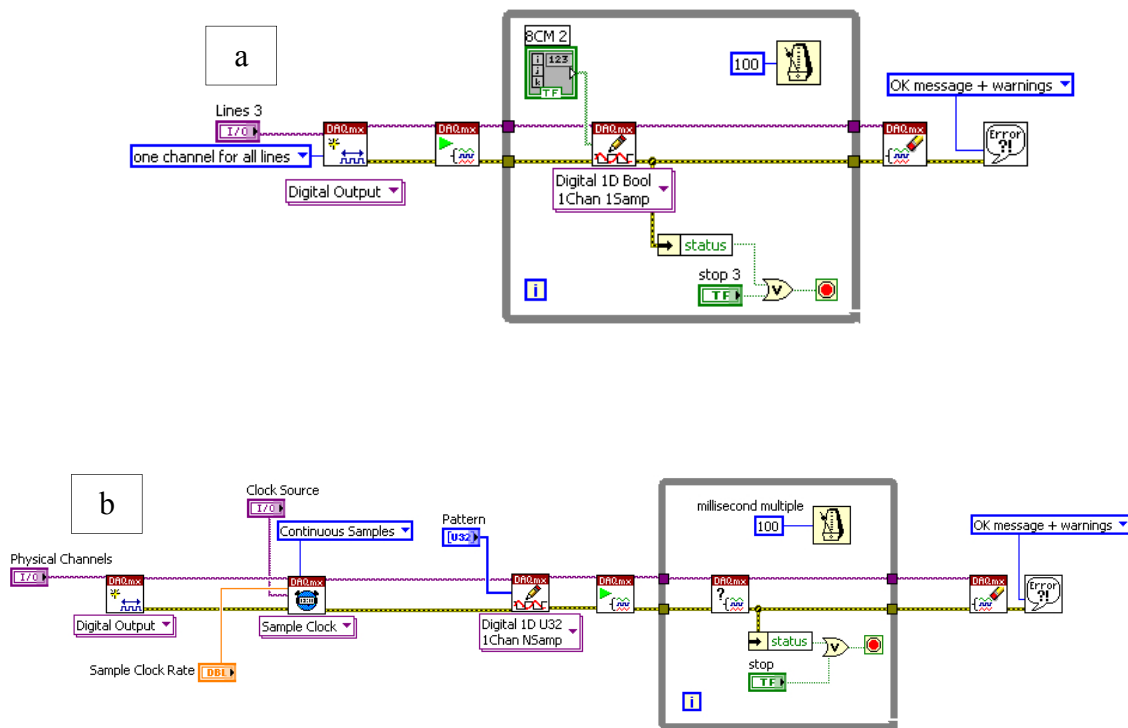


**Figure 3.9 :** Block diagrams of LabVIEW program utilized for operating the protein kinetics chip; (a) Valve control., (b) Mixer control

Also, this design allows us to operate the peristaltic pump in parallel with the operation of the valves. There is a separate switch, which allows us to turn on/off the pumping when needed during the device operation. All of the microfluidic operations described in section 3.1 can be easily performed by operating the respective valves controlled by LabVIEW<sup>®</sup> code.

### 3.6 DEVICE VALIDATION

The protein kinetics chip was mounted on an optical stereomicroscope (Carl Zeiss IMT Corporation), and images were captured using a PC-controlled color digital camera (Motic<sup>®</sup> Inc.). The mixer chip was operated by pneumatic control. A pressure of 15psi

was applied to the control channels for closing of the control valves and operation of mixer valves. To introduce fluids into the flow channels, a pressure of 5psi was applied to the dye solutions. The pneumatic control setup consists of three sets of eight-channel manifolds (Fluidigm<sup>®</sup> Corporation) controlled through a BOB3 control board (Fluidigm<sup>®</sup> Corporation). A digital I/O card (National Instruments<sup>®</sup>, PCI-6533) digitally mounted into the computer controlled the switching of each channel of manifolds through the BOB3 control board. A custom-built LabVIEW<sup>®</sup> (National Instruments) program was utilized for automatic control of individual valves. Figure 3.10 illustrates the schematic of the experimental setup utilized for validating the working of the protein kinetic chip.

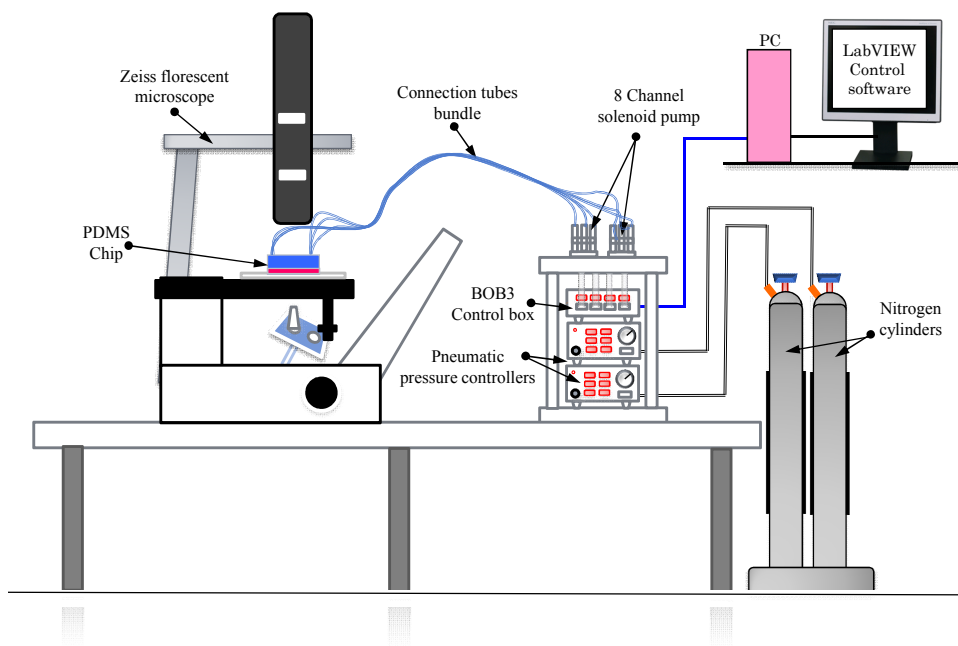


**Figure 3.10 :** Schematics of the experimental setup for validating the working of the protein kinetic chip.

Three food dyes of different colors were used during the validation of the operation of the

chip. The blue, red, and yellow dye colors represent dilution buffer, substrate, and enzyme, respectively. The three food dyes were pushed inside the mixer. Based on the captured images of the eleven mixers, performance of each mixer was quantified. Figure 3.11 shows the captured images of mixer numbers 1, 6 and 11.

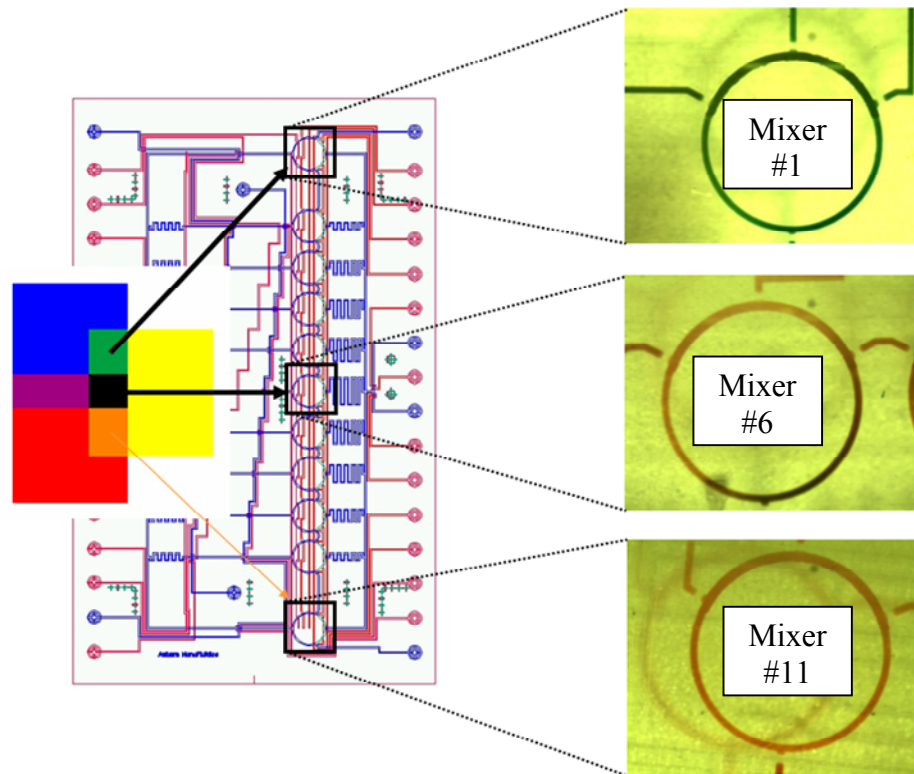


**Figure 3.11 :** The validation of chip operations by using blue, red and yellow colored food dye solutions.

In addition, these mixers illustrate three different mixed colors based on the respective amount of red, blue and yellow colored dyes present in them. Table 3.2 shows the summary of dye experiment conducted for validation of operation of the protein kinetics chip.



**Table 3.2 :** Summary of dye experiment for the validation of working of protein kinetics chip.

<b>Mixer No.</b>	<b>Dye color combination</b>	<b>Details about the mixer</b>
1	Blue+Yellow= Green	Negative control (No Substrate)
6	Blue+Red+Yellow=Black	50% Substrate: 50% Dilution buffer
11	Red+Yellow= Orange	Positive control (No dilution buffer)

### **3.7 CONCLUSION**

Highly integrated PDMS- based microfabricated devices that perform automated enzyme-catalyzed reactions, in parallel architecture assay format, were designed and developed. Active and precise microfluidic control of different colored food dye solutions was evaluated inside the chip. This was achieved by precise and swift functioning of microfluidic valves controls, fabricated by using multilayer soft lithography (MSL). A custom-built LabVIEW<sup>®</sup> program was developed and tested for computer control of the protein kinetic chip. Finally, the operational conditions were optimized for rapid and precise mixing operation inside the ring-shaped micro-mixers.

**CHAPTER FOUR**  
**PROTEIN KINETIC CHIP:**  
**DEVICE TESTING WITH A MODEL ENZYME SYSTEM**

**4.1 INTRODUCTION**

The successful validation of the protein kinetics chip could be further confirmed by conducting an enzyme-catalyzed assay. In this chapter, the testing of a model enzyme system in a protein kinetic chip is presented. In an ideal enzyme assay, a substrate concentration range is chosen to encompass values well above and below the approximate  $K_m$ . Design limitation of the device, on account of limited dilution ratios, could not follow this condition exactly while conducting the enzyme-catalyzed reaction on the chip.

**4.2 MODEL ENZYME SYSTEM**

**4.4.1 Restrictions on the selection of model enzyme system**

The choice of model enzyme for demonstrating chip based enzyme kinetics was limitless. However, the current protein kinetics chip design and optical detection system (ArrayWORX<sup>®</sup> biochip reader) restricted this choice to very few model enzymes. The requirements considered for selection of a model enzyme include the following:

- The model enzyme should be well-known for its application and well-studied among the enzyme kinetics research community.
- The model enzyme should have fluorescence-based detection. This was due to availability of a fluorescence-based detection system (ArrayWORX<sup>®</sup> biochip reader).
- The kinetics of the model enzyme should continue for at least a period of between 5 and 10 minutes in order to gather more data points for precise calculation of initial velocity for a suitable concentration range. For the given size of the chip, the scanning time inside the ArrayWORX<sup>®</sup> biochip reader takes a minimum of 30 seconds.

#### **4.4.2 LDH-Diaphorase model enzyme system**

As the first test subject, lactate dehydrogenase (LDH) was chosen as a model enzyme system because it exhibits kinetics towards substrates like lactate, which is very well-known because of its presence in wide variety of organisms including plants and animals and has commercially available substrates that are converted to fluorescent products. Though the conventional experiments with the LDH-diaphorase model enzyme system were successful, during the chip experiments we faced many challenges on account of its dual-step enzyme kinetics.

While the goal of measuring enzyme kinetics with the LDH-diaphorase model enzyme system on the chip was not successful, this stimulated consideration on alternative model enzymes. Work on the chip-based enzyme kinetics, first with LDH and later using

diaphorase, established a reliable on-chip method to conduct the chip experiments, culminating with the use of the  $\beta$ -galactosidase model enzyme system.

#### 4.4.3 $\beta$ -galactosidase model enzyme system

After encountering the limitations of the LDH-diaphorase model system,  $\beta$ -galactosidase ( $\beta$ -gal) was chosen as a model enzyme for demonstrating the enzyme-catalyzed reaction conducted on protein kinetics chip. The enzyme  $\beta$ -galactosidase breaks down the milk sugar lactose into simpler sugars *viz.*  $\beta$ -galactose and glucose. These sugar byproducts can be easily absorbed into the bloodstream. A large number of people around the world lack this enzyme, causing them to be lactose-intolerant. The milk industry uses  $\beta$ -galactosidase on a huge scale to produce lactose-free milk. When the small molecule resorufin  $\beta$ -D-galactopyranoside (RBG) is used as a  $\beta$ -gal substrate, the essentially non-fluorescent substrate is cleaved by  $\beta$ -gal to give up the products galactose and the red colored fluorescent dye resorufin (Hadd, Raymond *et al.* 1997). In this reaction, cleavage of RBG by  $\beta$ -gal is a single-step process that follows Michaelis-Menten kinetics (Hofmann and Sernetz 1984). The simple enzyme kinetics of the  $\beta$ -gal–RBG system, in addition to the fact that RBG is fluorogenic, makes this as an excellent model system (Seong, Heo *et al.* 2003). Figure 4.1 illustrates the  $\beta$ -gal enzyme catalyzed reaction. The conversion of RBG to resorufin occurs at excitation wavelength of  $\lambda_{ex} = 570$  nm, and emission wavelength  $\lambda_{em} = 590$  nm.

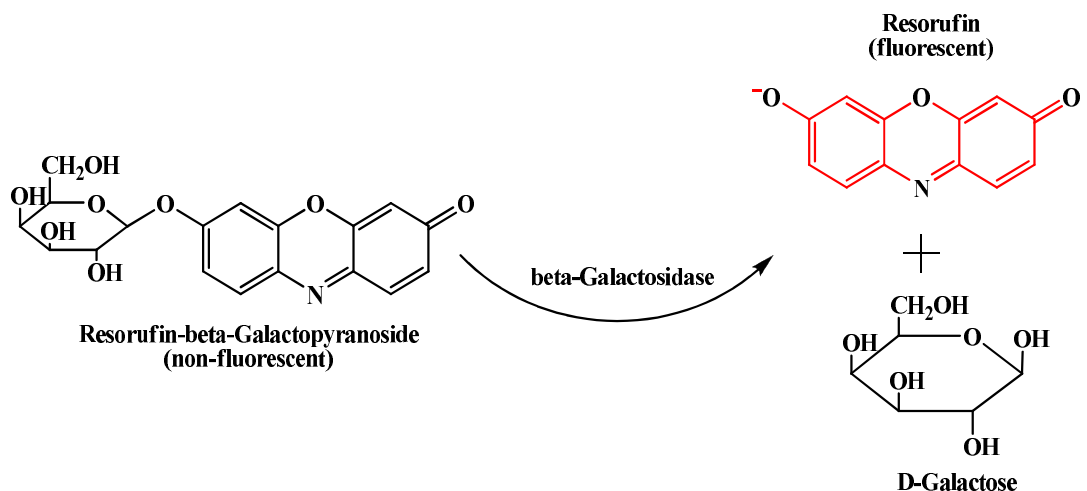


**Figure 4.1 :**  $\beta$ -Galactosidase enzyme-catalyzed reaction with Resorufin- $\beta$ -D-Galactopyranoside as substrate.

## 4.2 REAGENTS FOR CHIP TESTING

Resorufin (7-hydroxy-3H-phenoxazin-3-one),  $\beta$ -galactosidase ( $\beta$ -Gal, *Aspergillus oryzae*, 8 units/mg, 105 kDa), were purchased from Sigma (St. Louis, MO). Substrate resorufin  $\beta$ -D-galactopyranoside ( $\epsilon_{469} = 1.9 \times 10^4 \text{ L mol}^{-1} \text{ cm}^{-1}$ ) was obtained from Molecular Probes (Eugene, OR). All other chemicals were of analytical grade.

Dilution buffer was prepared from the mixture of Phosphate Buffered Saline (PBS) buffer (pH=7.4), 0.1% BSA,  $\text{MgCl}_2$  (1mM) and Tween solution (0.05%). Stock solutions of  $\beta$ -Gal, 0.0015 U/mL, and RBG, 333  $\mu\text{M}$ , were prepared in a PBS buffer. All the buffers were prepared with deionized water from Milli-Q filtration system (Millipore Co.).

**Table 4.1** Summary of reagents for protein kinetics chip testing.

Reagent	Description
Dilution buffer	PBS buffer (pH=7.4) + 0.1% BSA + $\text{MgCl}_2$ (1mM) + Tween solution (0.05%)
Substrate: resorufin $\beta$ -D-galactopyranoside	20 $\mu\text{M}$
Enzyme: $\beta$ -galactosidase	0.0003 U/mL

### 4.3 CHIP SCANNING

The protein kinetics chip was mounted on an optical microscope (Carl Zeiss IMT Corporation), and it was loaded with dilution buffer, substrate, and enzyme while on the microscope platform. The mixing process was conducted after placing the chip inside the ArrayWORX<sup>®</sup> biochip reader (Applied Precision<sup>®</sup>, LLC). The mixer chip was operated by pneumatic control. A pressure of 15psi was applied to the control channels for closing of the control valves and operation of mixer valves. To introduce dilution buffer, substrate, and enzyme into the flow channels, a pressure of 5psi was applied. The pneumatic control setup consists of four sets of eight-channel manifolds (Fluidigm<sup>®</sup> Corporation) controlled through a BOB3 control board (Fluidigm<sup>®</sup> Corporation) and fluidic pressure controllers (Fluidigm<sup>®</sup> Corporation). A digital PCI-6533 I/O card (National Instruments), mounted in a computer, digitally controls the switching of each channel of manifolds through the BOB3 control board. A custom-built LabVIEW<sup>®</sup> (National Instruments) program was utilized for automatic control of the individual valves. Figure 4.2 shows the schematics of the experimental set-up, in which the protein kinetic chip with the tubing connections was placed inside the ArrayWORX<sup>®</sup> biochip reader for the fluorescence scanning operation. Multiple images were captured during scanning of the chip by using a LINUX<sup>®</sup>-based PC connected to the ArrayWORX<sup>®</sup> biochip reader. The same computer was also employed for controlling the operation of the ArrayWORX<sup>®</sup> biochip reader.

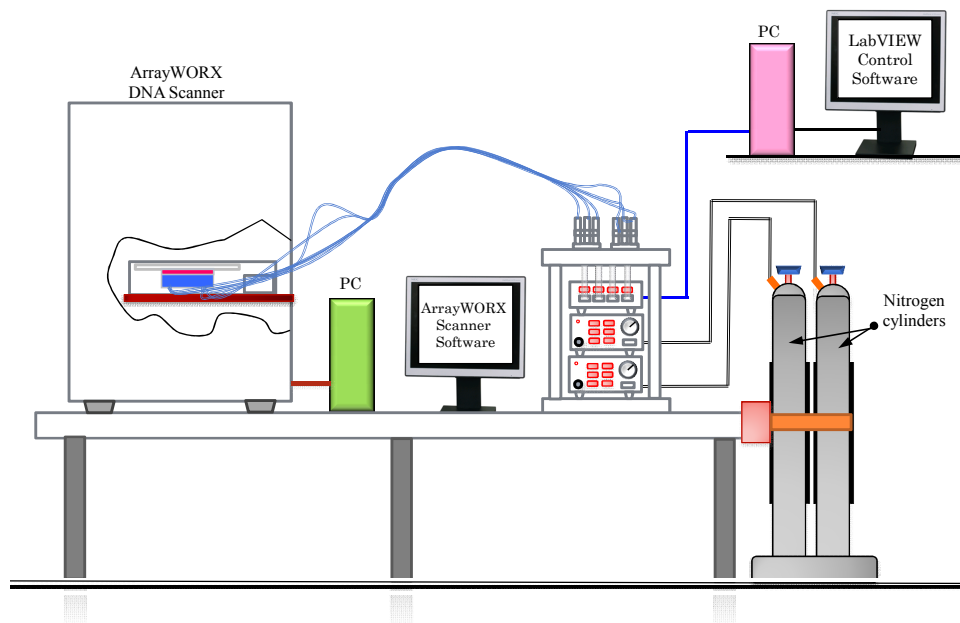


**Figure 4.2 :** Experimental set up for fluorescence scanning of the protein kinetics chip.

#### 4.4 DATA ANALYSIS

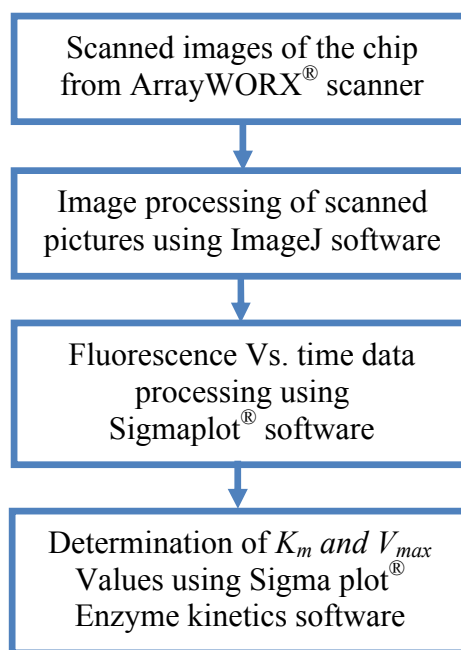


**Figure 4.3 :** Summary of steps followed during data analysis.

The steps followed during the data analysis of the chip-based enzyme-catalyzed reaction are given in Figure 4.3.

#### 4.4.1 Standard curve for resorufin

A standard curve is desired to calibrate the fluorescence data from the enzyme-catalyzed reaction. For the  $\beta$ -galactosidase-enzyme-catalyzed reaction, when the small molecule resorufin  $\beta$ -D-galactopyranoside (RBG) is used as a  $\beta$ -galactosidase substrate, essentially non-fluorescent substrate is cleaved by  $\beta$ -galactosidase to give up the products galactose and the red colored fluorescent dye resorufin (Hadd, Raymond *et al.* 1997). However, the fluorescence of resorufin emanating as product of the reaction needs to be calibrated with the standard curve obtained from pure resorufin.

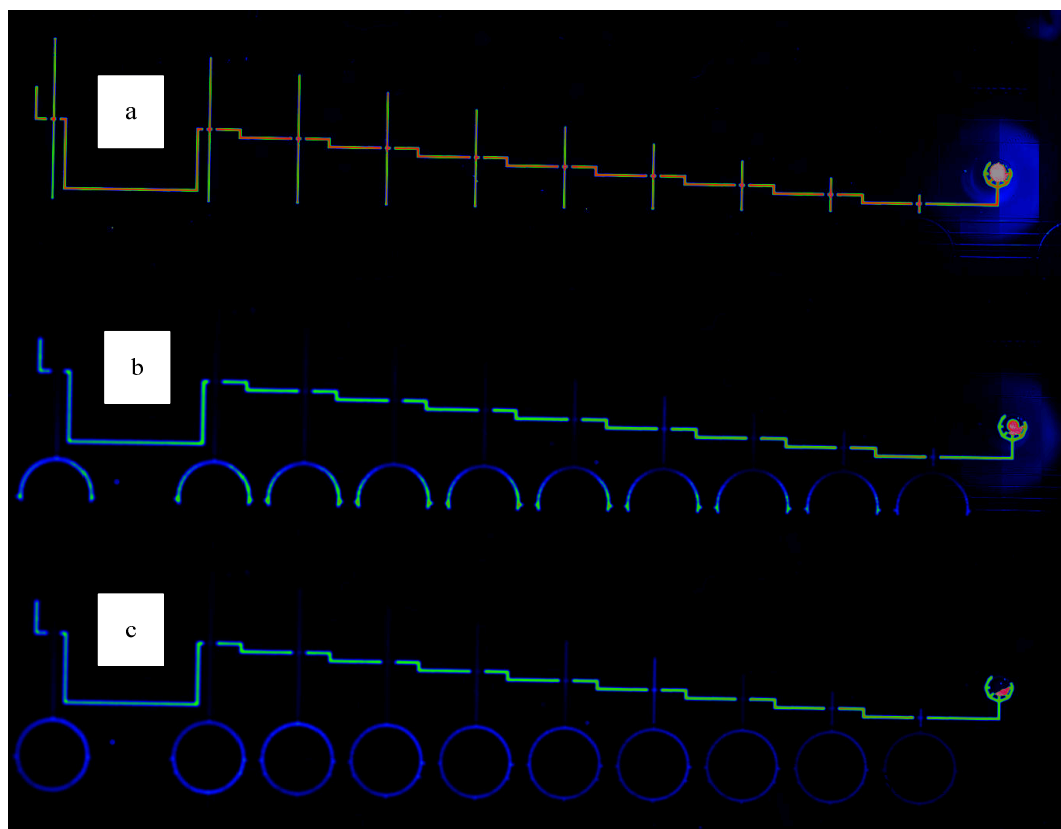


**Figure 4.4 :** Experiment for resorufin fluorescence standard curve ;(a),Resorufin fluorescence (b) Resorufin fluorescence gradient before mixing,(c) Final resorufin fluorescence gradient after the mixing.



As shown in Figure 4.4(a), the pure resorufin (Sigma-Aldrich, USA) was introduced through the substrate gradient part of protein kinetics chip. The dilution buffer was used for pushing the resorufin inside the mixer as illustrated in Figure 4.4(b). The figure also shows different amount of resorufin and dilution buffer present inside each mixer. Subsequently, through the enzyme part of the mixer, enzyme  $\beta$ -galactosidase was brought in, and the mixers were started. At the end of mixing, a gradient of fluorescence appeared from each mixer on account of different concentrations of resorufin present in them; this is depicted in Figure 4.4(c). By using the above mentioned procedure, the experiment was repeated five times, and the standard curve (Figure 4.5) was generated using the Systat Sigmaplot<sup>®</sup> Enzyme Kinetics module. However due to presence of back ground intensity the curve fitted line found to have y-intercept. To correct the problem of background intensity, the background intensity values are subtracted from each of the fluorescence intensity average values of different resorufin concentration. After this correction, the curve fitted line has y-intercept close to zero. In this plot, the line indicates curve-fitted standard curve, after the background intensity correction.

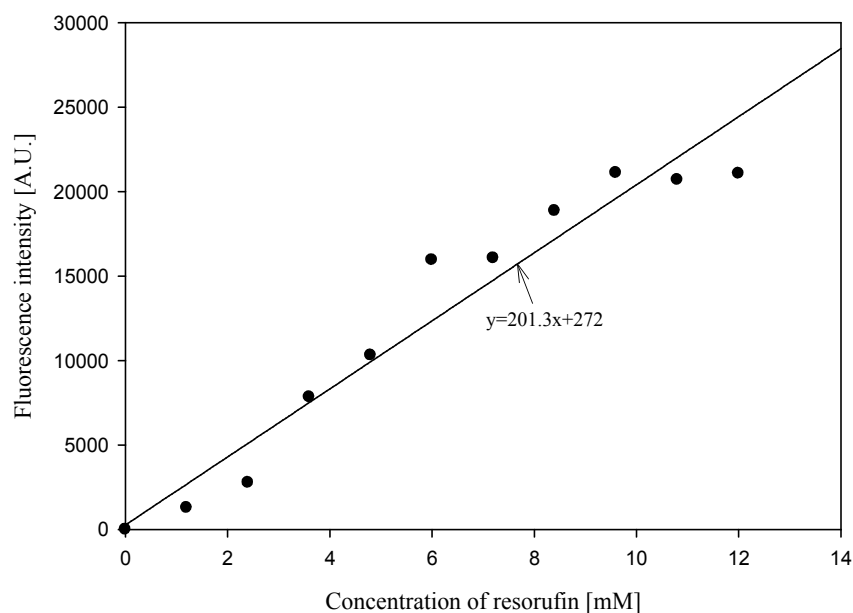


**Figure 4.5 :** Standard curve for resorufin generated by using protein kinetics chip.

#### 4.4.2 $\beta$ -galactosidase enzyme-catalyzed on-chip reaction

Following mixing of the dilution buffer,  $\beta$ -galactosidase and resorufin  $\beta$ -D-galactopyranoside (RBG), the chip was scanned as mentioned in section 4.3. The scanned pictures were transferred to ImageJ<sup>®</sup> software for further image processing. Figure 4.6 demonstrates the array of scanned pictures captured at different time scans from 0 to 1960 sec. In the array of pictures, zero fluorescence was observed in ring mixer number 0 (negative control) through all the time scans, while maximum fluorescence was noticed in ring mixer number 10 (positive control). In the rest of the ring mixers, the fluorescence observed was expected considering the volume of dilution buffer,  $\beta$ -gal enzyme and RBG substrate present in each.

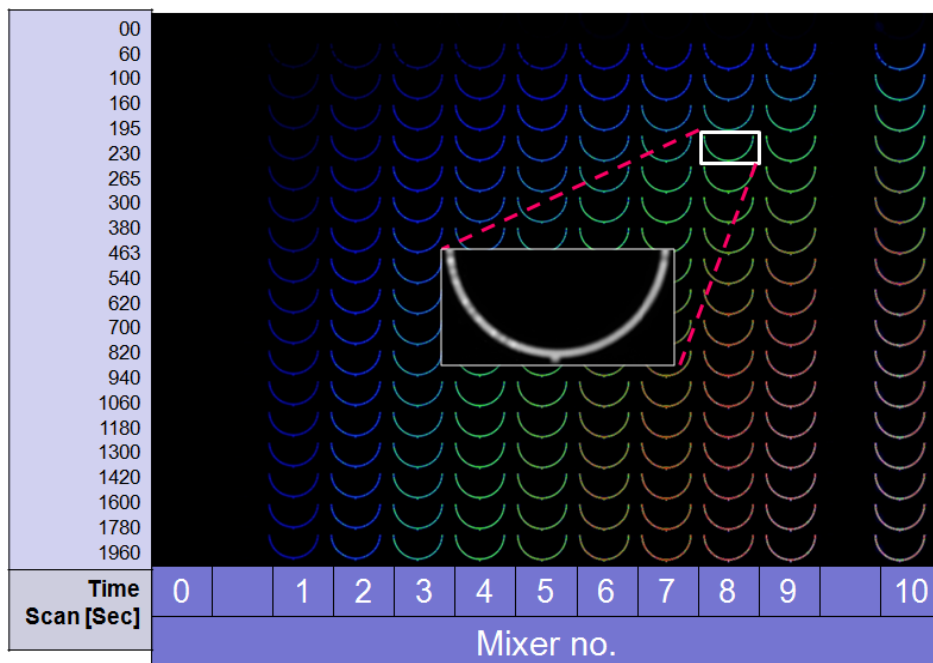


**Figure 4.6 :** Array of scanned pictures generated by scanning the protein kinetics chip.

The picture at each time scan was converted into fluorescence intensity data by analyzing multiples of region of interests (ROI's). This tabular data included time and fluorescence intensity for each ring mixer. Figure 4.7 graphically represents the results of the image processing.

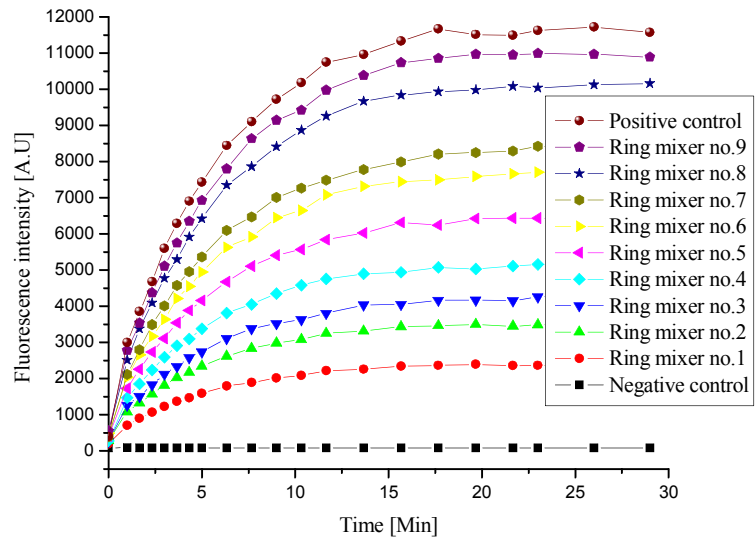


**Figure 4.7 :** Time history for  $\beta$ -galactosidase enzyme obtained by using protein kinetics chip.

From the Figure 4.7, it is clear that the  $\beta$ -gal enzyme saturates the RBG substrate after approximately 18 minutes.

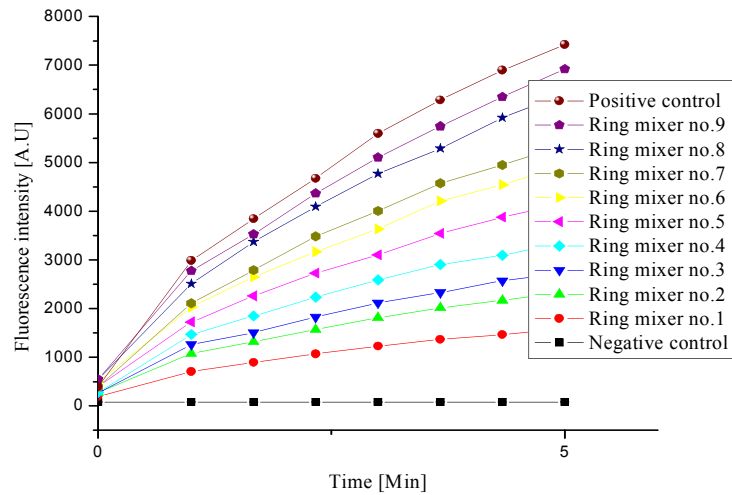


**Figure 4.8 :** Time history in linear kinetics range for  $\beta$ -galactosidase enzyme obtained by using protein kinetics chip.

In Figure 4.8, the initial region between 0 and 1 minute was dedicated for the mixing and burst process also. For the evaluation of initial velocities of the reactions, the region from 0 to 1 minute was considered for each ring mixer. The chip experiment was repeated twice, and the evaluated initial velocity with respect to substrate concentration was plotted as shown in Figure 4.9. The difference in the initial velocity was attributed to lack of reproducibility of experiment in the microfluidic chip due to protein absorption to the channel walls. The absorption of the protein to the channel walls is a challenging problem and needs to be addressed separately.

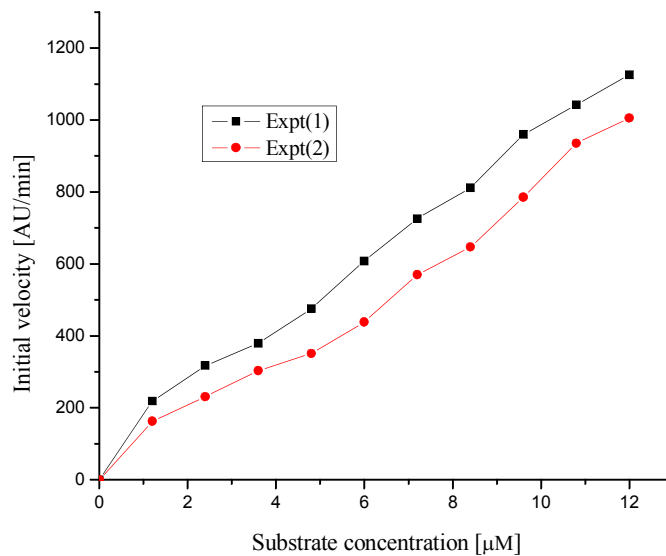


**Figure 4.9 :** Initial velocity plot for  $\beta$ -galactosidase enzyme obtained by using protein kinetics chip.

#### 4.5 RESULTS

The initial velocity and the substrate concentration data were transferred to the Systat Sigmaplot<sup>®</sup> Enzyme Kinetics module. The curve-fitting of the data was carried out in the same program by using Michaelis-Menten equation. The Michaelis-Menten plot and Lineweaver-Burk plot are given in Figure 4.10 and Figure 4.11, respectively.

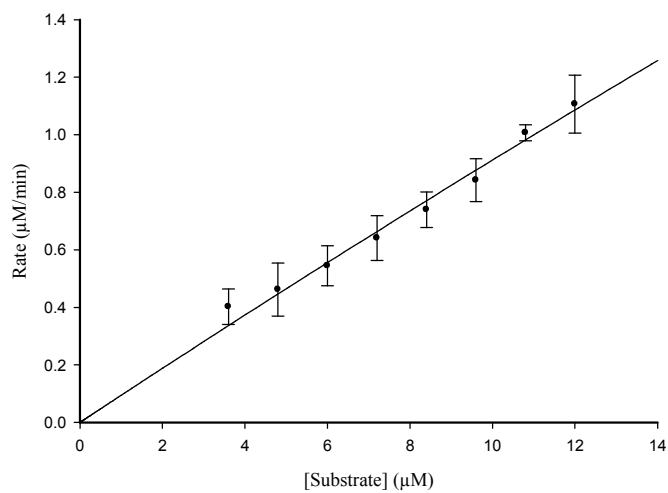


**Figure 4.10 :** Michaelis-Menten plot for  $\beta$ -galactosidase enzyme by using protein kinetics chip.

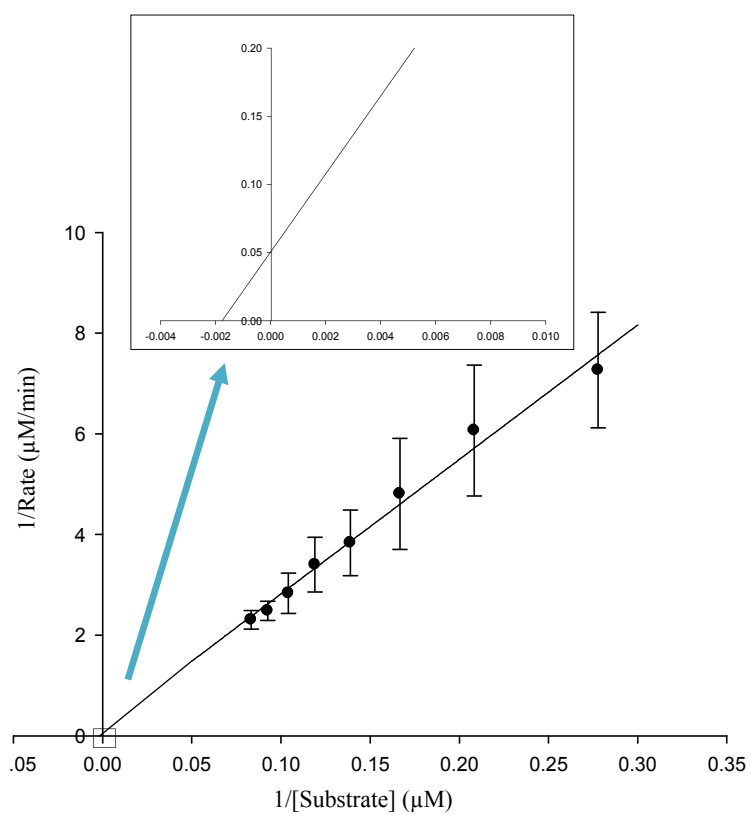


**Figure 4.11:** Lineweaver-Burk plot for  $\beta$ -galactosidase enzyme by using protein kinetics chip.

Table 4.2 represents the summary of curve-fitting and kinetic parameters obtained from Sysstat Sigmaplot<sup>®</sup> Enzyme Kinetics module for  $\beta$ -galactosidase enzyme.

**Table 4.2** Summary of curve-fitting of  $\beta$ -galactosidase enzymatic reaction in order to determine kinetic parameters for  $\beta$ -galactosidase on-chip experiment

Parameter	Value
$K_m$ [ $\mu\text{M}$ ]	473
Standard deviation for $K_m$ [ $\mu\text{M}$ ]	$\pm 462$
$k_{cat}$ [ $\text{min}^{-1}$ ]	48711
Standard deviation for $k_{cat}$ [ $\text{min}^{-1}$ ]	$\pm 4871$
Goodness of fit in terms of $R^2$	0.9275

Table 4.3 presents a summary of kinetic parameters obtained from the protein kinetics chip experiment for  $\beta$ -galactosidase enzyme and their comparison with literature values for same model enzyme system.

**Table 4.3** Summary of kinetic parameters for  $\beta$ -galactosidase enzyme.

	$K_m$ [ $\mu\text{M}$ ]	$k_{cat}$ [ $\text{min}^{-1}$ ]	Source
Protein kinetic chip	$473 \pm 462$	$48711 \pm 4871$	-
Literature values	$550 \pm 200$	$43800 \pm 4380$	(Hofmann and Sernetz 1984),(Hadd, Raymond <i>et al.</i> 1997),
Conventional experiment in the AU campus	$85 \pm 38$	$40920 \pm 8132$	

## 4.6 CONCLUSION

Considering the limitation of the chip design and optical scanning system, we encountered difficulty in selection of a model enzyme system for testing the functionality of the protein kinetic chip. Progress in the chip-based enzyme-catalyzed experiment was



initiated by using LDH-diaphorase model enzyme system. However LDH-diaphorase system failed to demonstrate the working of protein kinetics chip due to its dual-step kinetics. Ultimately,  $\beta$ -galactosidase was chosen as a model enzyme on the basis of its simplicity, its single-step kinetics, and the availability of sensitive, fluorescence-based substrates. From table 4.3, it was observed that the values of  $K_m$  and  $k_{cat}$  seem to match appreciably with the literature values. These kinetic constants were determined by curve-fitting the data points in Lineweaver-Burk plot. Here two data points, with the low substrate concentration, were not considered during the curve-fitting, on account of excessive deviation from the linear behavior. It was also observed that the Michaelis-Menten plot appeared different than the typical hyperbolic curve. This appears to represent first-order kinetics for lower-substrate concentrations of the Michaelis-Menten plot. Consequently it was not possible to determine the values of kinetic constants from curve-fitting of Michaelis-Menten equation. The reason for uncommon Michaelis-Menten plot could be attributed to narrow substrate concentration, i.e.,  $[S] \ll K_m$  ( $\sim 550 \pm 200$ ), and to the availability of few data points for curve-fitting. While problems such as the deviation of the Michaelis-Menten plot than the typical hyperbolic curve reduced the utility of the protein kinetics chip, the results from Lineweaver-Burk show promising potential of the device.

#### **4.7 SCIENTIFIC ISSUES**

Improvements in areas such as chip design, with much wider dilution ratios encompassing substrate concentration well-distributed above and below the value of  $K_m$

for a given enzyme system, and modification and development of dedicated optical detection systems could surely improve the working of protein kinetic chip more exhaustively and precisely. The protein kinetics chip can be modified using a more widely distributed dilution ratios such as 1:2, 1:4, 1:8, 1:16, 1:32, 1:64, 1:128, 1:256, 1:512, 1:1024, and 1:2048 and/or additional number of parallel processors. Widely distributed dilution ratios would have the capability of encompassing the substrate concentration range well above and below the value of  $K_m$  for enzyme under investigation. While this might also lead to accomplish both the first-order and zeroth-order kinetics for the enzyme, making the investigation of enzyme complete. The additional number of processors would provide more data points to improve the quality of curve fitting and arrive at correct values of kinetic constants.

In addition, the protein kinetics chip can be integrated with an optical detection system and temperature control system for rapid detection and for conducting enzyme kinetic experiments at various temperatures. The integrated microfluidic platform may certainly extend the range of investigation of enzymes, with very fast millisecond kinetics, for the study. The need for incubating the enzymes during reaction and the capability for conducting enzymatic reactions at multiple temperatures should also be addressed.

## CHAPTER FIVE

### OVERALL CONCLUSIONS

#### 5.1 CONCLUSIONS OF THE RESEARCH

1. A complicated protein kinetics microfluidic platform is successfully developed by means of a range of interdisciplinary tools and techniques. Major tools and techniques involved in the development process include mechanical design, computer aided drafting (CAD), microfabrication, soft lithography, LabVIEW<sup>®</sup> control, and enzyme kinetics.
2. The enzyme  $\beta$ -galactosidase ( $\beta$ -gal)/resorufin- $\beta$ -galactopyranoside (RBG) model enzyme system was successfully tested on a protein kinetics chip. From these experiments, it was observed that, the values of  $K_m$  and  $k_{cat}$  seem to match considerably with the literature values. It was also observed that the Michaelis-Menten plot appeared different than the typical hyperbolic curve. This appears to indicate first order kinetics part for lower-substrate concentrations of the Michaelis-Menten plot.

3. The parallel processing of polymer-based microfluidic platform containing a ring mixer is extended to eleven parallel processors. Based on the author's knowledge, the current state of parallel processing in the area of microfluidics is found to be maximized at three parallel processors
4. A generalized LabVIEW<sup>®</sup> program for microfluidic valve and peristaltic mixer operation is developed. This program could be utilized for multitudes of microfluidic platforms for various applications.

## REFERNECES

- Balagadde, F. K., H. Song, et al. (2008). "A synthetic Escherichia coli predator-prey ecosystem." Mol Syst Biol **4**: 1-8.
- Bugg, T. D. H. (2004). An Introduction to Enzyme and Coenzyme Chemistry Blackwell Publishers.
- Chou, H., M. Unger, et al. (2001). "A Microfabricated Rotary Pump." Biomedical Microdevices **3**(4): 323-330.
- Chou, H. P., M. A. Unger, et al. (2001). "A Microfabricated Rotary Pump." Biomedical Microdevices, **3**(4): 323-330.
- Cornish-Bowden, A. (1995). Analysis of Enzyme Kinetic Data, Oxford University Press.
- Cornish-Bowden, A. (2004). Fundamentals of Enzyme Kinetics Portland Press.
- Daw, R. and J. Finkelstein (2006). "Lab on a chip." Nature **442**(7101): 367-367.
- Dettmer, S. (2001-2004). "Sara Dettmer performing enzyme kinetics research." from <http://www.adrian.edu/chemistry/th/Students/2001-2004%20students/students2001-2004.php>.
- Fu, A. Y., H. P. Chou, et al. (2002). "An Integrated Microfabricated Cell Sorter." Anal. Chem. **74**(11): 2451-2457.
- Gomez-Sjoberg, R., A. A. Leyrat, et al. (2007). "Versatile, Fully Automated, Microfluidic Cell Culture System." Anal. Chem. **79**(22): 8557-8563.
- Hadd, A. G., D. E. Raymond, et al. (1997). "Microchip Device for Performing Enzyme Assays." Anal. Chem. **69**(17): 3407-3412.
- Haeberle, S. and R. Zengerle (2007). "Microfluidic platforms for lab-on-a-chip applications." LAB ON A CHIP **7**(9): 1094-1110.

- Hansen, C. L., E. Skordalakes, et al. (2002). "A robust and scalable microfluidic metering method that allows protein crystal growth by free interface diffusion." Proceedings of the National Academy of Sciences **99**(26): 16531-16536.
- Hofmann, J. and M. Sernetz (1984). "Immobilized enzyme kinetics analyzed by flow-through microfluorimetry : Resorufin-[beta]-galactopyranoside as a New Fluorogenic Substrate for [beta]-Galactosidase." Analytica Chimica Acta **163**: 67-72.
- Hong, J. W., V. Studer, et al. (2004). "A nanoliter-scale nucleic acid processor with parallel architecture." Nat Biotech **22**(4): 435-439.
- Hruby, J. (2001). "LIGA technologies and applications." MRS Bulletin: 337-340.
- Kahane, L. H. (2008). Regression basics, Sage Publications, Inc.
- Kamholz, A. E. (2004). "Proliferation of microfluidics in literature and intellectual property." Lab on a Chip **4**(2): 16N-20N.
- Kang, J. H. and J.-K. Park (2005). "Development of a microplate reader compatible microfluidic device for enzyme assay." Sensors and Actuators B: Chemical **107**(2): 980-985.
- Kartalov, E. P., A. Scherer, et al. (2007). "Experimentally validated quantitative linear model for the device physics of elastomeric microfluidic valves." Journal of Applied Physics **101**(6): 064505-4.
- Kern, W. (1993). Handbook of Semiconductor Cleaning Technology. Park Ridge, NJ, Noyes Publishing:
- Kern, W. and J. Vossen (1978). Thin Film Processes. New York, Academic Press:
- Lin, C. H., G. B. Lee, et al. (2002). "A new fabrication process for ultra-thick microfluidic microstructures utilizing SU-8 photoresist." J. Micromech. Microeng. **12**: 590-597.
- Madou, M. J. (1998). Fundamentals of Microfabrication, CRC-Press.
- Mantle, T. J. (2001). "Enzymes: nature's nanomachines. Royal Irish Academy Medal Lecture." Biochem. Soc. Trans. **29**(Pt 2): 331-336.
- Marangoni, A. G. (2002). Enzyme Kinetics: A Modern Approach, Wiley-Interscience.

- McDonald, J. C., D. C. Duffy, et al. (2000). "Fabrication of microfluidic systems in poly(dimethylsiloxane)." Electrophoresis **21**(1): 27-40.
- Nguyen, N.-T. and S. T. Wereley (2006). Fundamentals And Applications of Microfluidics, Artech House Publishers.
- Nguyen, N. and Z. Wu (2005). "Micromixers - a review." JOURNAL OF MICROMECHANICS AND MICROENGINEERING **15**(2): R1-R16.
- Oddy, M., J. Santiago, et al. (2001). "Electrokinetic instability micromixing." ANALYTICAL CHEMISTRY **73**(24): 5822-5832.
- Palmer, T. (1995). Understanding Enzymes, Prentice Hall.
- Piribo (2006). Strategic Report on Enzymes: US industry forecasts to 2010 & 2015.
- Reyes, D. R., D. Iossifidis, et al. (2002). "Micro total analysis systems. 1. Introduction, theory, and technology." Anal Chem. **74**(12): 2623-36.
- Seong, G. H., J. Heo, et al. (2003). "Measurement of Enzyme Kinetics Using a Continuous-Flow Microfluidic System." Anal. Chem. **75**(13): 3161-3167.
- Song, H., D. L. Chen, et al. (2006). "Reactions in Droplets in Microfluidic Channels." Angewandte Chemie International Edition **45**(44): 7336-7356.
- Song, H. and R. F. Ismagilov (2003). "Millisecond Kinetics on a Microfluidic Chip Using Nanoliters of Reagents." J. Am. Chem. Soc. **125**(47): 14613-14619.
- Squires, T. M. and S. R. Quake (2005). "Microfluidics: Fluid physics at the nanoliter scale." Reviews of Modern Physics **77**(3): 977-50.
- Srinivasan, V., V. K. Pamula, et al. (2004). "Droplet-based microfluidic lab-on-a-chip for glucose detection." Analytica Chimica Acta **507**(1): 145-150.
- Stroock, A., S. Dertinger, et al. (2002). "Chaotic mixer for microchannels." SCIENCE **295**(5555): 647-651.
- Studer, V., G. Hang, et al. (2004). "Scaling properties of a low-actuation pressure microfluidic valve." Journal of Applied Physics **95**(1): 393-398.
- Tai, C. H., R. J. Yang, et al. (2006). "Micromixer utilizing electrokinetic instability-induced shedding effect." Electrophoresis **27**(24): 4982-4990.
- Unger, M. A., H.-P. Chou, et al. (2000). "Monolithic Microfabricated Valves and Pumps by Multilayer Soft Lithography." Science **288**(5463): 113-116.

- Urban, P. L., D. M. Goodall, et al. (2006). "Enzymatic microreactors in chemical analysis and kinetic studies." Biotechnology Advances **24**(1): 42-57.
- Warren, L., D. Bryder, et al. (2006). "Transcription factor profiling in individual hematopoietic progenitors by digital RT-PCR." Proceedings of the National Academy of Sciences **103**(47): 17807-17812.
- Whitesides, G. M. (2006). "The origins and the future of microfluidics." Nature **442**(7101): 368-373.
- Xia, Y. and G. M. Whitesides (1998). "Soft Lithography." Annual Review of Materials Science **28**(1): 153-184.
- Young, I. T., R. Moerman, et al. (2003). "Monitoring enzymatic reactions in nanolitre wells." Journal of Microscopy **212**: 254-263.



## APPENDIX-A

### REAGENT PREPARATION

#### Buffer stock solutions

Phosphate buffered saline, pH7.4	1x concentration
Tween-20	1x concentration
Bovine serum albumin (BSA)	1x concentration
MgCl <sub>2</sub> (1M)	1 M

#### Reaction buffer mixture

		Final concentration
99.85 mL	Phosphate buffered saline, pH7.4	0.01 M
0.05 mL	Tween-20	0.05 %(v/v)
0.1 g	Bovine serum albumin (BSA)	0.1 %(w/v)
0.1 mL	MgCl <sub>2</sub> (1M)	1 mM

#### Substrate stock solutions

Dilution buffer	1x concentration
Resorufin $\beta$ -D-galactopyranoside	33 mM

#### Substrate mixture

		Final concentration
990 $\mu$ L	Dilution buffer	-
10 $\mu$ L	Resorufin $\beta$ -D-galactopyranoside	330 $\mu$ M

**Enzyme stock solutions**

Dilution buffer	1x concentration
$\beta$ -galactosidase	50 U/mL

**Enzyme mixture**

990 $\mu$ L	Reaction buffer	Final concentration
10 $\mu$ L	$\beta$ -galactosidase	-
		0.5 U/mL

**APPENDIX-B**  
**DATA PROCESSING FOR CONVENTIONAL**  
**EXPERIMENT**

**Time history of enzyme product formation for  $\beta$ -galactosidase and resorufin  $\beta$ -D-galactopyranoside enzyme-catalyzed conventional experiment**

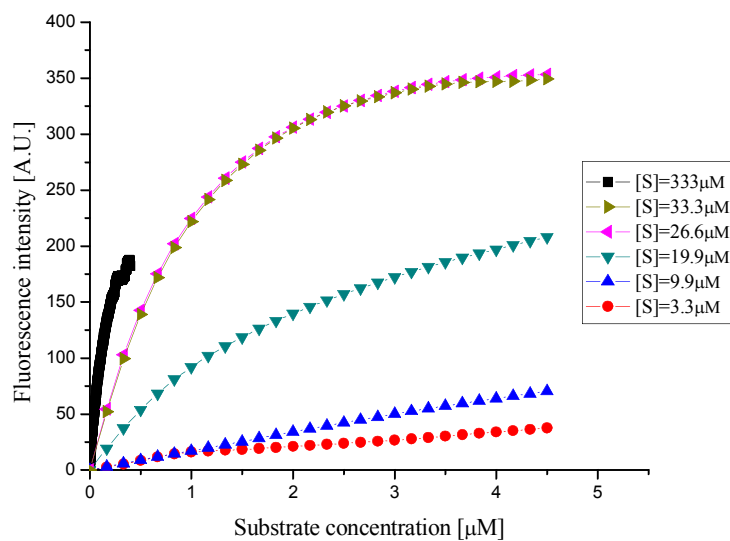


**Figure:** Time history plot for  $\beta$ -galactosidase enzyme kinetics experiment obtained by conventional method.

**Velocities obtained from time history of conventional experiment**

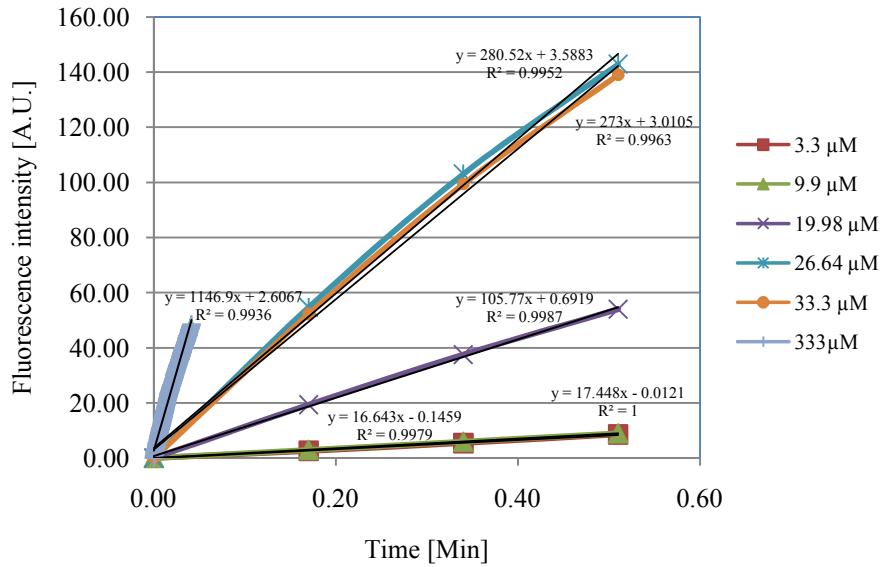


**Figure:** Velocities for  $\beta$ -galactosidase enzyme kinetics experiment obtained by conventional method for substrate concentration experiment

**Standard curve for resorufin fluorescence conventional experiment**

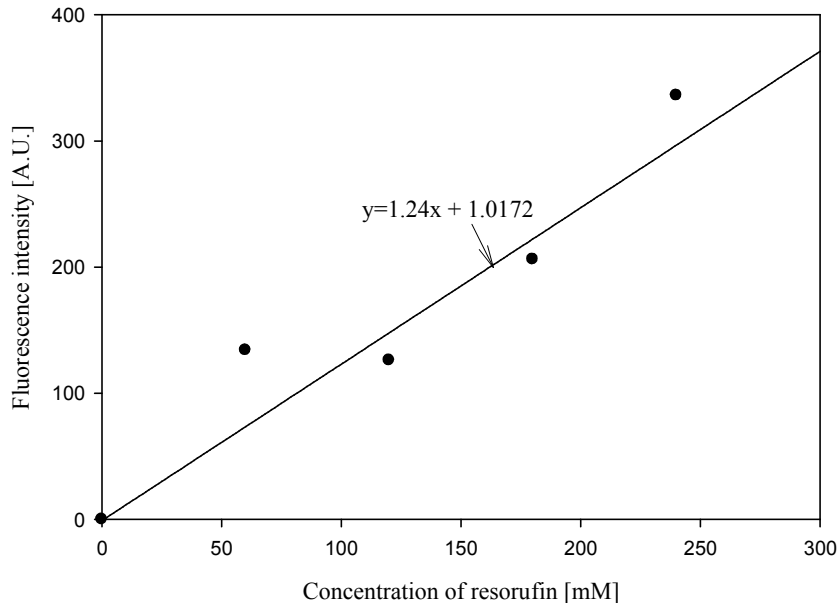


**Figure:** Standard curve for resorufin generated by using conventional experiment.

### Michaelis-Menten plot for $\beta$ -galactosidase enzyme-

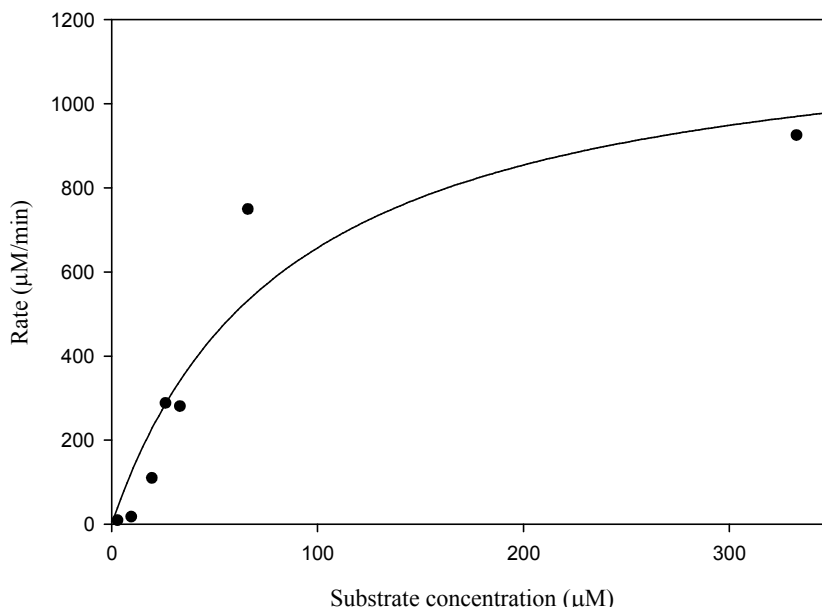


**Figure:** Michaelis-Menten plot for  $\beta$ -galactosidase enzyme by using conventional experiment.

### Data analysis for the determination of kinetic constants

**Table** Summary of curve-fitting of  $\beta$ -galactosidase enzymatic reaction in order to determine kinetic parameters for  $\beta$ -galactosidase conventional experiment

Parameter	Value
$K_m$	$85 \pm 38$
$V_{max}$	$1218 \pm 242$
Goodness of fit in terms of $R^2$	0.8962

#### a. Determination of $V_{max}$

$$V_{max} = 1218 \pm 242 \mu\text{M}/\text{min}$$

#### b. Determination of $K_m$

$$K_m = 85 \pm 38 \mu\text{M}$$

**c. Determination of  $k_{cat}$**

Concentration of  $\beta$ -galactosidase from *Aspergillus oryzae* = 8 U/mg

Amount of  $\beta$ -galactosidase from *Aspergillus oryzae* used during assay = 0.025 U/mL

Therefore, amount of  $\beta$ -galactosidase used during assay =  $3.125 \times 10^{-3}$  mg/mL

Molecular weight of  $\beta$ -galactosidase from *Aspergillus oryzae* = 105 kDa

$$\mu\text{mole/mL of enzyme used} = \frac{\text{mg/mL of enzyme}}{\text{protein concentration (kDa)} \times 10^3 \frac{\text{mg}}{\text{g}} \times 10^{-6} \frac{\text{mole}}{\mu\text{mole}}}$$

$$\mu\text{mole/mL of enzyme used} = \frac{3.125 \times 10^{-3} \frac{\text{mg}}{\text{mL}}}{105 (\text{kDa}) \times 10^3 \frac{\text{mg}}{\text{g}} \times 10^{-6} \frac{\text{mole}}{\mu\text{mole}}}$$

$$\mu \frac{\text{mole}}{\text{mL}} \text{ of enzyme used} = 29.76 \times 10^{-3}$$

Therefore

$$k_{cat} = \frac{V_{max} \mu\text{mole} \cdot \text{mL}^{-1} \cdot \text{min}^{-1}}{[E] \mu\text{mole} \cdot \text{mL}^{-1}}$$

$$k_{cat} = \frac{1218 \pm 242 \mu\text{mole} \cdot \text{mL}^{-1} \cdot \text{min}^{-1}}{29.76 \times 10^{-3} \mu\text{mole} \cdot \text{mL}^{-1}}$$

$$= 40920 \pm 8132 \text{ min}^{-1}$$

$$= 682 \pm 136 \text{ sec}^{-1}$$

**APPENDIX-C**  
**DATA PROCESSING FOR ON-CHIP**  
**EXPERIMENT**

**Time history of enzyme product formation for  $\beta$ -gal and resorufin- $\beta$ -D-galactopyranoside enzyme-catalyzed on-chip experiment –**

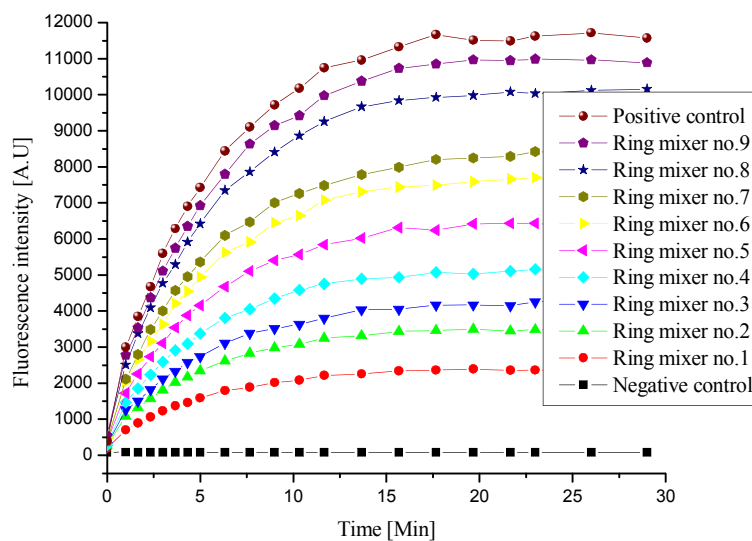


**Figure:** Time history plot for  $\beta$ -galactosidase enzyme kinetics experiment obtained by on-chip for experiment no.1.

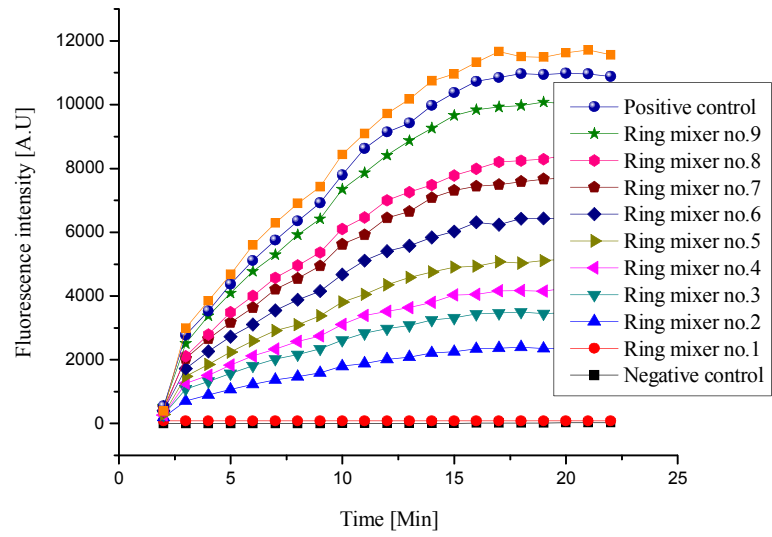


**Figure:** Time history plot for  $\beta$ -galactosidase enzyme kinetics experiment obtained by on-chip for experiment no.2.



**Velocities obtained from time history of conventional experiment-**

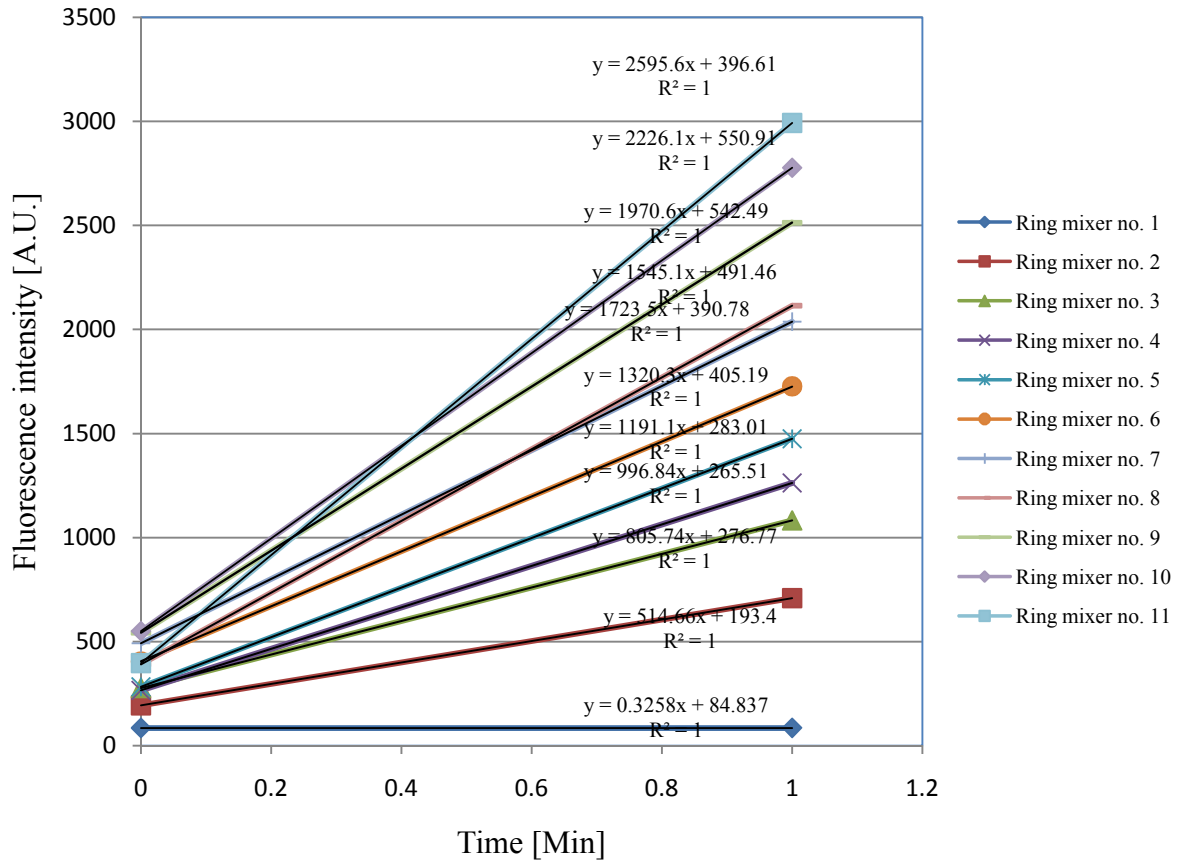


**Figure:** Velocities for  $\beta$ -galactosidase enzyme kinetics experiment obtained by on-chip for experiment no.2.

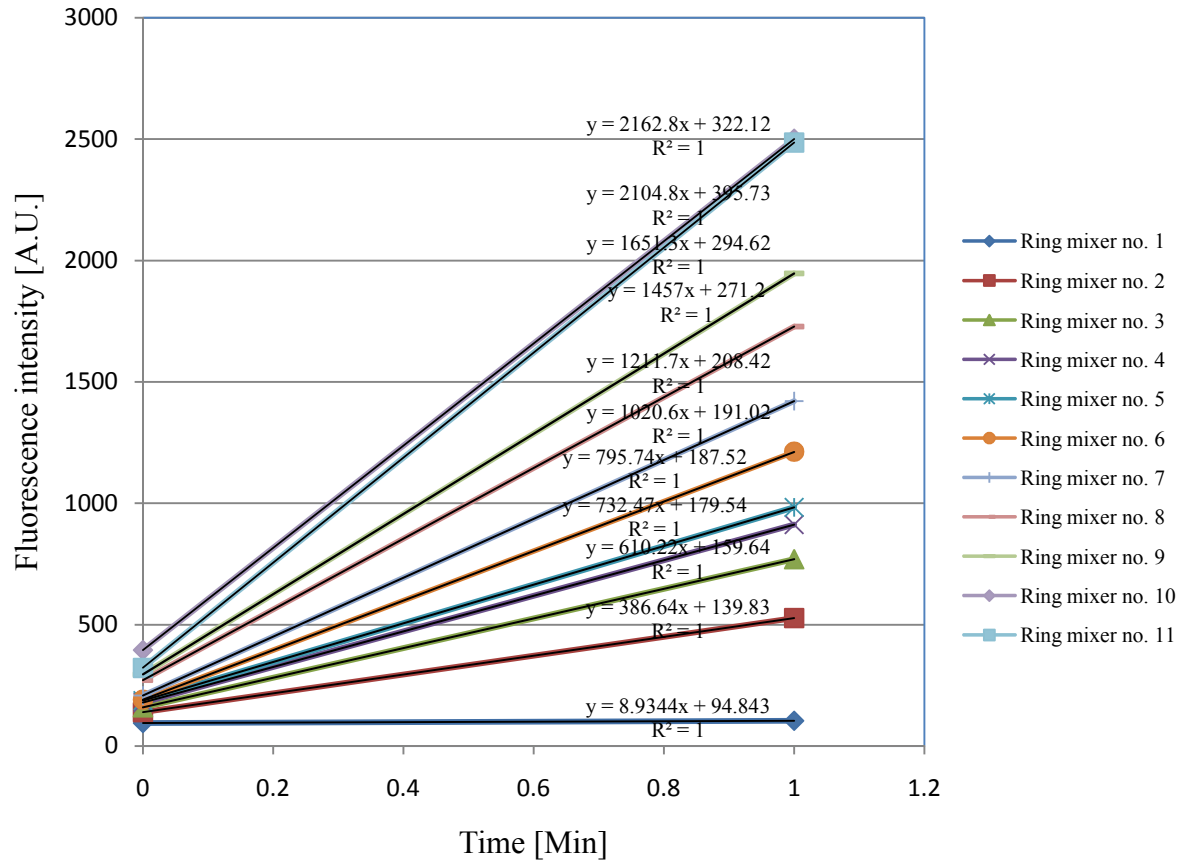


**Figure:** Velocities for  $\beta$ -galactosidase enzyme kinetics experiment obtained by on-chip for experiment no.2.

### Standard curve for resorufin fluorescence conventional experiment-

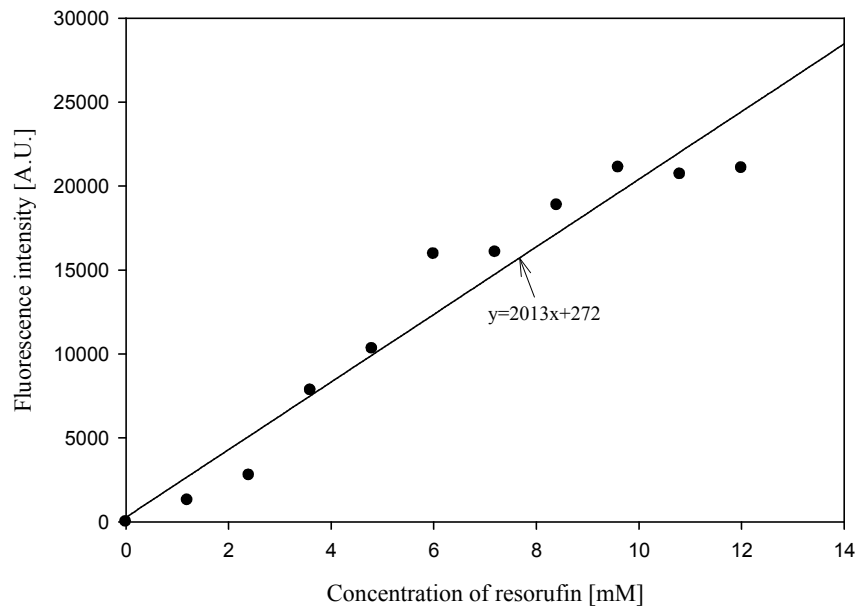


**Figure:** Standard curve for resorufin generated by using on-chip experiment.

### Lineweaver-Burk plot for $\beta$ -galactosidase enzyme-

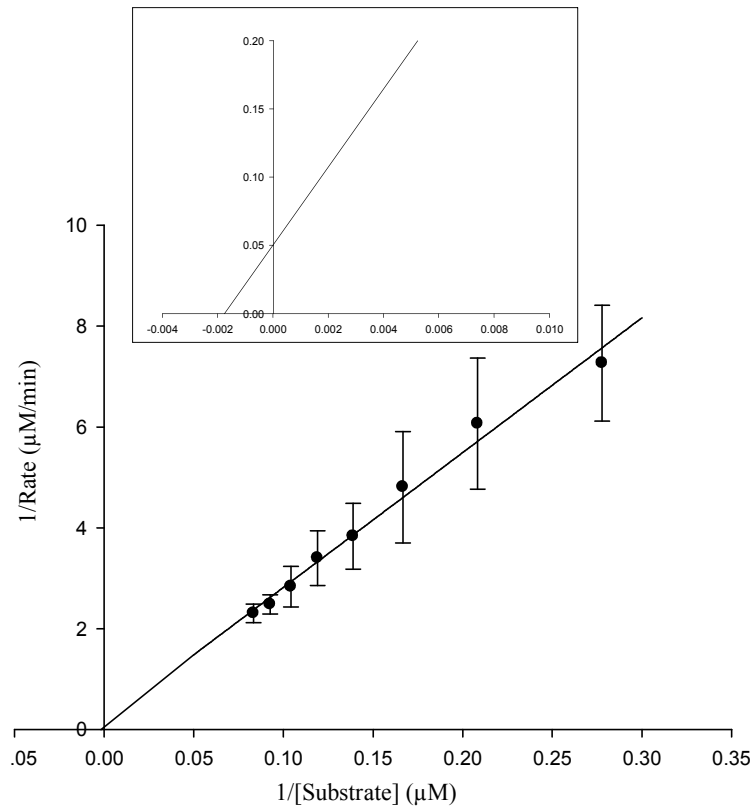


**Figure:** Lineweaver-Burk plot for  $\beta$ -galactosidase enzyme by using on-chip experiment.

### Data analysis for the determination of kinetic constants-

**Table** Summary of curve-fitting of enzymatic reaction in order to determine kinetic parameters for  $\beta$ -galactosidase on-chip experiment

Parameter	Value
x-intercept	$-(0.0029 \pm 0.00216)$
y-intercept	$0.0575 \pm 0.00575$
Goodness of fit in terms of $R^2$	0.9275

#### d. Determination of $V_{max}$ –

$$V_{\max} = \frac{1}{y_0} = \frac{1}{0.0575 \pm 0.00575}$$

$$\therefore V_{\max} = 17.39 \pm 1.739 \text{ } \mu\text{M}/\text{min}$$

**e. Determination of  $K_m$  –**

$$K_m = -(0.0029 \pm 0.00216)$$

$$\therefore K_m = 473 \pm 462 \text{ } \mu\text{M}$$

**f. Determination of  $k_{cat}$  –**

Concentration of  $\beta$ -galactosidase from *Aspergillus oryzae* = 8 U/mg

Amount of  $\beta$ -galactosidase from *Aspergillus oryzae* used during assay = 0.0003 U/mL

Therefore, amount of  $\beta$ -galactosidase used during assay =  $3.75 \times 10^{-5}$  mg/mL

Molecular weight of  $\beta$ -galactosidase from *Aspergillus oryzae* = 105 kDa

$$\mu\text{mole}/\text{mL of enzyme used} = \frac{\text{mg}/\text{mL of enzyme}}{\text{protein concentration}(\text{kDa}) \times 10^3 \frac{\text{mg}}{\text{g}} \times 10^{-6} \frac{\text{mole}}{\mu\text{mole}}}$$

$$\mu\text{mole}/\text{mL of enzyme used} = \frac{3.75 \times 10^{-5} \frac{\text{mg}}{\text{mL}}}{105(\text{kDa}) \times 10^3 \frac{\text{mg}}{\text{g}} \times 10^{-6} \frac{\text{mole}}{\mu\text{mole}}}$$

$$\mu\text{mole}/\text{mL of enzyme used} = 3.57 \times 10^{-4}$$

Therefore

$$k_{cat} = \frac{V_{\max} \mu\text{mole} \cdot \text{mL}^{-1} \cdot \text{min}^{-1}}{[E] \mu\text{mole} \cdot \text{mL}^{-1}}$$

$$k_{cat} = \frac{17.39 \pm 1.739 \mu\text{mole} \cdot \text{mL}^{-1} \cdot \text{min}^{-1}}{3.57 \times 10^{-4} \mu\text{mole} \cdot \text{mL}^{-1}}$$

$$= 48711 \pm 4871 \text{ min}^{-1}$$

$$= 811 \pm 81.1 \text{ sec}^{-1}$$